Investigation of Structure, Dynamics, and Solvation in 1-Octanol and Its Water-Saturated Solution: Molecular Dynamics and Free-Energy Perturbation Studies

Stephen E. DeBolt* and Peter A. Kollman

Contribution from the Department of Pharmaceutical Chemistry, University of California, San Francisco, California 94143

Received April 6, 1994[⊗]

Abstract: We have carried out molecular dynamics studies of 1-octanol and its water-saturated solution using a slightly modified version of the OPLS (optimized intermolecular potential function for liquid simulations) model. The structural, dynamic, and energetic properties of these systems were studied via molecular dynamics simulations and compared with experiment where possible. The structure of the pure liquid and solutions are characterized in terms of fluctuating regions of preferentially polar and nonpolar character, including inverted micellar aggregates. Calculations of the dielectric constant and three dielectric relaxation times of 1-octanol give reasonable agreement with experiment. The results of time-correlation analyses performed on MD trajectory data are appraised with respect to the various explanations proposed by experimentalists for the multiple-frequency dielectric responses observed in 1-octanol. We propose a mechanism (involving the turnover of hydrogen-bonded aggregates) for the less well-understood low-frequency dielectric response. We have computed the relative partition coefficients of benzene and phenol in pure water versus hydrated 1-octanol in quantitative agreement with experiment. Here, by analyzing octanol/water solvation-shell structuring around the solutes, insight is gained into hydrated 1-octanol's capability to serve as a biophase analog.

I. Introduction

A detailed understanding of the interactions of solutes such as drugs, metabolites, ionophores, and peptides with aqueous versus lipidic body tissues could help to direct rational drug design strategies. It has been shown that some common clinical drugs can interact very specifically with biomembranes[1,2] while enroute to or possibly even while associating with a protein target site. Computer simulations could provide a valuable source of molecular-level information concerning interaction specificities. But, even with current supercomputers, it is difficult to simulate dynamic membrane-bilayer/solute systems at the level of atomic detail over extensive time spans. It would be beneficial to thoroughly examine a simpler model system possessing molecular traits which are analogous to those of biomembranes and proteins.

The octanol/water partitioning system has become the standard reference for investigating the compartmental distribution characteristics of pharmaceutical agents.[3-5] It is also sometimes used to predict pharmacokinetic characteristics of drug compounds in the biophases. Why does octanol serve as such a remarkably good experimental model for reproducing the partitioning behavior of drugs in body tissues? Octanol is commonly regarded as a simple isotropic bulk solvent, essentially hydrophobic or "oily". But, water/oil partitioning studies have shown that, when a strict hydrocarbon (instead of say octanol or olive oil) is chosen as the "oil" phase, correlations between partitioning behavior and biological activity break down.[3,6,7] 1-Octanol shares the traits of amphiphilicity and hydrogen-bonding capability with the phospholipids and proteins found in biological membranes. It is a structural analog for phospholipids in particular, with its polar "head group" and flexible nonpolar "tail". In this paper, we have used computer simulations to clarify the means by which the amphiphilic nature of the octanol molecule gives rise to distinctive internal structuring in the media, enabling it to serve as a biophase model.

Given the fundamental role that octanol plays in drug partitioning studies and the fact that it is probably the best simple model for an amphiphilic lipid, it is surprising that no definitive molecular-modeling simulations have been carried out on this system. Part of the reason for this is the difficulty in ensuring convergence for computed properties in viscous and mixed systems. There have been several molecular-level simulations involving alkanes, alkanols, fatty acid chains, or micelles,[8-12] and several simulations of small bilayer "patches".[13-17] Even

* Current address: The Scripps Research Institute, 10666 North Torrey Pines Road, Department of Molecular Biology, MB1, La Jolla, CA 92037.

⊗ Abstract published in *Advance ACS Abstracts,* May 1, 1995.

(1) Mason, R. P.; Rhodes, D. G.; Herbette, L. G. *J. Med. Chem.* **1991**, *34*, 867-77.

(2) Herbette, L. G.; Trumbore, M.; Chester, D. W.; Katz, A. M. *J. Mol. Cell. Cardiol.* **1988**, *20*, 373-378.

(3) Smith, R. N.; Hansch, C.; Ames, M. M. *J. Pharm. Sci.* **1975**, *64*, 599.

(4) Leo, A.; Hansch, C.; Elkins, D. *Chem. Rev.* **1971**, *71*, 525.

(5) Hansch, C.; Leo, A. J. *Substituent Constants for Correlation Analysis in Chemistry and Biology*; Wiley: New York, 1979. Hansch, C.; Dunn, W. J. *J. Pharm. Sci.* **1972**, *61*, 1.

(6) Flynn, G. L. *J. Pharm. Sci.* **1971**, *60*, 345.

(7) Burton, D. E.; Clarke, K.; Gray, G. W. *J. Chem. Soc.* **1964**, 1314.

(8) Wendoloski, J. J.; Kimatian, S. J.; Schutt, C. E.; Salemme, F. R. *Science* **1989**, *243*, 636.

(9) Karaborni, S.; O'Connell, J. P. *J. Phys. Chem.* **1990**, *94*, 2624. Karaborni, S.; O'Connell, J. P. *Langmuir* **1990**, *6*, 905.

(10) Watanabe, K.; Klein, M. L. *J. Phys. Chem.* **1989**, *93*, 6897.

(11) Shelley, J.; Watanabe, K.; Klein, M. L. *Int. J. Quantum Chem., Quantum Biol. Symp.* **1990**, *17*, 103-117.

(12) Jonsson, B.; Edholm, O.; Teleman, O. *J. Chem. Phys.* **1986**, *85*, 2259.

(13) Damodaran, K. V.; Merz, K. M. *Langmuir* **1993**, *9*, 1179-83. Damodaran, K. V.; Merz, K. M.; Gaber, B. P. *Biochemistry* **1992**, *31*, 7656.

(14) McKinnon, S. J.; Whittenburg, S. L.; Brooks, B. R. *J. Phys. Chem.* **1992**, *96*, 10497.

(15) Egberts, E.; Berendsen, H. J. C. *J. Chem. Phys.* **1988**, *89*, 3718. van der Ploeg, P.; Berendsen, H. J. C. *J. Chem. Phys.* **1982**, *76*, 3271; *Mol. Phys.* **1983**, *49*, 233.

0002-7863/95/1517-5316$09.00/0

the slowest relaxation time of pure or water-saturated octanol is orders of magnitude more rapid than some slow phenomena observed in lipid membranes. But the relatively slow dynamic reorientational events occurring in 1-octanol converge much less rapidly than analogous events in, say, pure water.

A first goal of this study was to reproduce the structural and thermodynamic properties of liquid 1-octanol and its water-saturated solution and to provide a complete molecular-level characterization of its internal microstructure, polymeric hydrogen-bonding, polar/nonpolar clustering, and dynamic reorientation. The structurophysical properties of the media were well reproduced. The important role played by saturating waters in octanol's internal structure becomes clear on analysis of the MD trajectory. Further, these studies reveal the molecular-level details of the structural microheterogeneity and dynamics of the media.

Fundamental microwave and infrared spectroscopy studies first indicated the presence of hydrogen-bonded polymeric entities in pure 1-octanol media, leading experimentalists[18] to postulate the presence of long linear open chains of varying lengths as well as multimeric closed-ring structures. We explore the following question: is there a link between 1-octanol's local structural anisotropy and its dielectric response behavior?

The internal dynamics of octanol media are also of interest as pharmacokinetic parameters involving transport are sometimes predicted from octanol/water partitioning studies.[19,20] The qualitatively correct relative trends in the relevant dynamic properties are reproduced, although in their absolute magnitudes the dynamics are consistently too rapid, probably due to the absence of explicit hydrogens in the united atom model.

The feasibility of reproducing octanol/water partition coefficients via the free-energy perturbation (FEP) methodology are examined. A coarse-grain parallel FEP computing regime was successfully instituted and demonstrated excellent promise in this regard. The difference in octanol/water transfer free energies was calculated for two small solutes, benzene and phenol. Agreement with the experimentally determined value is excellent. Detailed structural information was obtained regarding the specific molecular-level interactions responsible for differences in the partition coefficients of these molecules.

II. Methodology

A. Molecular Mechanics and Dynamics: Energy Functions and Protocols. One of the most successful models of molecular liquids using a simple potential energy function is OPLS. In particular, there are OPLS parameters for liquid short-chain alkanes and alcohols[21] which demonstrate the capability of this model to reproduce experimentally observable thermodynamic liquid properties. Hydrocarbon molecules are modeled using the "united atom" approach, where alkyl hydrogens are included implicitly. The appropriate Fourier torsion terms are added to model the hydrogen-to-hydrogen 1−4 interactions by appropriately parameterizing the H−C−C−H dihedral rotational energies. OPLS hydrocarbon and alkoxyl models were adapted for use in AMBER MM/MD,[22] with some notable parameter modifications required.

1. Adaptation of OPLS/MC Parameters to AMBER/MD. The original OPLS potential energy function was parameterized assuming rigid bonds and angles as implemented for Monte Carlo (MC) simulations. However, we wished to allow bond angle flexibility within MD. Secondly, the OPLS potential energy function differs from AMBER's in its use of *different* sets of nonbonded (Lennard-Jones type) parameters σ and ϵ for inter- versus intramolecular interactions, where intramolecular involves atoms separated by more than three bonds.[21] AMBER's potential energy function uses the *same* van der Waals (VDW) parameters for *both* inter- and intramolecular nonbonded interactions but provides a scaling factor which can be used to attenuate intramolecular 1−4 interactions. The influence of intramolecular angle deformability must be considered in parameterizing AMBER's torsional parameters; the rigid rotor approximation is not imposed here. In view of these differences between molecular models and functional representations, one would not necessarily expect the OPLS/MC parameters to transfer directly to AMBER/MD without modification. Indeed, initial MD simulations using *unmodified* OPLS parameters did not reproduce the correct experimental liquid densities and heats of vaporization as accurately as the OPLS/MC results.

The intermolecular nonbonded and electrostatic interaction terms, analogous in both force fields, were adopted unchanged from the OPLS to the AMBER force field with a single exception. The nonbonded well-depth parameter ϵ (kcal/mol) for the methyl group was slightly decreased for long-chain hydrocarbons. Because there are fewer nonbonded interactions and torsion angles involving methyl than methylene groups in hexane, octane, and octanol, modification of the ϵ(methyl) rather than the ϵ(methylene) caused the least perturbation of the original OPLS model. After fitting the torsional potentials to the best available data, this modification of ϵ(methyl) brought about the best obtainable simultaneous reproduction of experimental observables for hexane, i.e., chain conformer distribution, liquid density, and heat of vaporization.

Values of σ identical to OPLS methylene and methyl groups (where $\sigma = 2^{1/6}R^*$) and ϵ(methylene) = 0.118 kcal/mol were used here. But, setting ϵ(methyl) to 0.150 kcal/mol gave closer agreement with experimental data for hexane. In trial parameterization runs, the ϵ-(methyl) parameter was varied over the range 0.12−0.19, in pure liquid hexane at 298 K, using isothermal isobaric (NTP) ensembles with periodic boundary conditions. Each 300 ps trial parameterization run was started from a previously aged liquid hexane box using ϵ(methyl) equal to (the OPLS value) 0.175 kcal/mol; data were collected after the first 50 ps of each run. A previous MD simulation[23] of rigid three-point methanol demonstrated the transferability of OPLS intermolecular hydroxyl parameters from MC to MD.

It was necessary to fit AMBER's intramolecular terms to those of the OPLS potential energy function (which was designed to faithfully reproduce the energies of 91 monomer conformational states by mimicking Allinger's MM2 force field, which very closely reproduces experimental data).[21,24] For the organic liquids simulated in the current study (hexane, octane, 1-octanol, and 1-octanol/water), the OPLS geometries[21] (also see Table 2) were adopted and AMBER's angle bending force constants were employed, angles remaining free to bend. Bond lengths were constrained via the SHAKE algorithm.[25] The alkane

(16) Edholm, O.; Johansson, J. *Eur. Biophys. J.* **1987**, *14*, 203.

(17) Stouch, T. R.; Alper, H. E.; Bassolinoklimas, D. *Int. J. Supercomput. Appl. High Perform. Comput.* **1994**, *8*, 6−23. Bassolino-Klimas, D.; Alper, H. E.; Stouch, T. R. *Biochemistry* **1993**, *32*, 12624. Alper, H. E.; Bassolinoklimas, D.; Stouch, T. R. *J. Chem. Phys.* **1993**, *99*, 5547. Stouch, T. R. *Molecular Simulation* **1993**, *10*, 335. Alper, H. E.; Bassolinoklimas, D.; Stouch, T. R. *J. Chem. Phys.* **1993**, *98*, 9798.

(18) Oster, G.; Kirkwood, J. G. *J. Chem. Phys.* **1943**, *11*, 175. Smyth, C. P. *Dielectric Behavior and Structure*; McGraw Hill Book Co., Inc.: New York, 1955. Piekara, A. *J. Chem. Phys.* **1961**, *36*, 2145. Van Ness, H. C.; Van Winkle, J.; Richtol, H. H.; Hollinger, H. B. *J. Phys. Chem.* **1967**, *71*, 1483. Johari, G. P.; Dannhauser, W. *J. Chem. Phys.* **1968**, *48*, 5114. Tucker, E. E.; Becker, E. D. *J. Phys. Chem.* **1973**, *77*, 1783. Campbell, C.; Brink, G.; Glasser, L. *J. Chem. Phys.* **1975**, *79*, 660.

(19) Betageri, G. V.; Rogers, J. A. *Pharm. Rev.* **1989**, *6*, 399.

(20) Gaspari, F.; Bonati, M. *J. Pharm. Pharmacol.* **1987**, *39*, 252.

(21) Jorgensen, W. L. *J. Phys. Chem.* **1986**, *90*, 1276. Jorgensen, W. L.; Madura, J. D.; Swenson, C. J. *J. Am. Chem. Soc.* **1984**, *106*, 6638. Jorgensen, W. L. *J. Chem. Phys.* **1983**, *87*, 5304.

(22) Weiner, S. J.; Kollman, P. A.; Nguyen, D. T.; Case, D. A. *J. Comput. Chem.* **1986**, *7*, 230. Weiner, S. J.; Kollman, P. A.; Case, D. A.; Singh, U. C.; Ghio, C. C.; Alagona, G.; Profeta, S., Jr.; Weiner, P. *J. Am. Chem. Soc.* **1984**, *106*, 765. Pearlman, D. A.; Case, D. A.; Caldwell, J. W.; Seibel, G. L.; Singh, U. C.; Weiner, P. K.; Kollman, P. A. *AMBER (UCSF)*, version 4.0; Department of Pharmaceutical Chemistry, University of California: San Francisco, CA, 1991. In the AMBER molecular mechanical potential function H_{Total} is the potential energy of a system of atoms composed in terms of the following component energies: harmonic bond and bond-angle stretching about a given equilibrium value, a fourier torsional angle term, and for nonbonded particles, pairwise Lennard-Jones 6−12 and Coulombic interactions, and an optional 10−12 hydrogen-bonding term.

(23) DeBolt, S. E.; Kollman, P. A. *J. Am. Chem. Soc.* **1990**, *112*, 7515.

(24) Burkert, U.; Allinger, N. *Molecular Mechanics*; American Chemical Society: Washington, DC, 1982.

(25) van Gunsteren, W. F.; Berendsen, H. J. C. *Mol. Phys.* **1977**, *34*, 1311. Ryckaert, J. P.; Ciccotti, G.; Berendsen, H. J. C. *J. Comput. Phys.* **1977**, *34*, 327. Ciccotti, G.; Ferrario, M.; Ryckaert, J. P. *Mol. Phys.* **1982**, *47*, 1253.

torsion parameters were determined by first fitting a two-term Fourier potential so the shape of the 3-fold rotational potential presented by Jorgensen[21] was closely reproduced in an isolated hexane monomer. From this point of reference, slight modifications were made (as necessary because flexible angle bending was permitted) so that the results of liquid hexane simulations optimally agreed with experimental hexane conformer distributions.[26] After systematic searches over several trial parameter combinations in liquid MD simulations, the best value found for the 1−4 intramolecular VDW scale factor was 1/7.4 (essentially the same as determined by Jorgensen and Tirado Rives (1/8) for the OPLS/AMBER force field[27]). This value was used in all simulations discussed in this study.

Initial configurations were prepared by placing molecules at evenly spaced lattice points within the appropriate volume space, then randomly displacing within a tolerance zone (0.5 Å) along all three axes, and randomly rotating (0−360 degrees) about each axis. Cubic periodic boxes of 125 molecules (hexane and octane), 250 molecules (1-octanol), or 304 molecules (water-saturated 1-octanol), were used in the simulations. The NTP (constant temperature (298 K), pressure (1 bar), and composition) MD systems were minimized, then extensively relaxed. A modified Verlet dynamics algorithm, commonly referred to as the leap-frog method was used to solve the equations of motion.[28] Temperature and pressure were held constant via the Berendsen algorithm for coupling to an external bath.[29] Relaxation proceeded until monotonic limiting values were reached for density, internal energy, temperature, and pressure, and beyond this to a total of 500 ps for hexane and 1.0 ns for octane and octanol. The binary octanol/water system was not used in parameter fitting.

The same relaxation criteria were followed for 40 °C and 75 °C 1-octanol simulations, but the pre-equilibrated 25 °C system was used as their starting configuration. These higher temperature systems, one near human body temperature and one higher still, ensured rapid enough internal reorientations to facilitate the study of dynamical phenomena and media reconfiguration over a computationally accessible time span.

2. Fitting Criteria. The fitting criteria were the liquid densities (hexane, octane, and 1-octanol), heats of vaporization (hexane, octane, and 1-octanol), and liquid-phase molecular conformer distribution (hexane). The density, ϱ, is available from a constant-temperature, constant-pressure MD simulation as the molecular weight of N molecules divided by the time ensemble average volume of the periodic box.

$$\varrho = \frac{\text{mass}_N}{\langle \text{volume} \rangle_{\text{box}}} \quad (1)$$

The heat of vaporization can be determined as (given that $\Delta H = \Delta E_i + P\Delta V$ at constant P)

$$\Delta H_{\text{vap}} = (E_{\text{inter}}(\text{g}) - E_{\text{inter}}(\text{l})) + (E_{\text{intra}}(\text{g}) - E_{\text{intra}}(\text{l})) + RT \quad (2)$$

where E_{inter} is the internal energy of the interacting liquid molecules (the intermolecular VDW and electrostatic terms in AMBER), E_{intra}, the intramolecular energy (bonds, angles, torsions, and intramolecular VDW and electrostatic terms) for the liquid, is subtracted from the gas value, R is the gas constant, and T is the temperature. Assuming an ideal gas, $E_{\text{inter}}(\text{g})$ for the gas phase is approximated as zero, and the RT term substitutes for $P\Delta V$, the work of expansion, in the constant-pressure enthalpy change equation. $E_{\text{intra}}(\text{g})$ values for the gases were determined from an average of multiple molecular dynamics simulations of the isolated monomers summing to a time span of 2 ns (hexane and octane) or 4 ns (octanol). After initial liquid relaxations, liquid-phase fitting criteria were evaluated by averaging over at least three MD runs of 100 ps for hexane, 200 ps for octane, and 300 ps for octanol.

3. Fitting to Conformer Distributions. The model was fit to definitive experimental data regarding the conformational distribution of chain molecules. Wong, Mantsch, and Snyder (WMS) used rotational isomeric state (RIS) models to assign Raman spectroscopy bands to specific conformers of *n*-hexane.[26] While the use of RIS[30] analysis (a rudimentary theoretical method for determining the distribution frequencies among a set of available conformational states by using their Boltzman probabilities) is not strictly an "experimental" technique, WMS were able to achieve good qualitative agreement when assigning experimentally determined Raman signals to hexane's set of RIS conformational states. Their conclusions conceming the conformational distribution are dependent on the uncertain magnitude of the gauche/trans energy difference chosen as an RIS parameter. WMS present data for two possible energy differences, 0.5 and 0.9 kcal/mol. In Table 1, their findings for the percentages of each conformer are compared to those generated by our final set of AMBER/MD liquid alkane parameters. The final AMBER/MD long-chain alkane/alkanol parameters are given in Table 2.

Table 1. Hexane Conformational Data

confn	WMS RIS[a] ($\Delta E = 0.5$)	WMS RIS ($\Delta E = 0.9$)	AMBER/MD
ttt	18.9	36.1	39.2
gtt	32.7	31.9	24.2
tgt	16.4	16.0	13.7
gtg	14.2	7.0	13.6
ggt	15.6	7.9	7.5
ggg	3.3	1.0	1.9

	outer angles[b]	inner angle
exptl (WMS $\Delta E = 0.5$)		
gauche	41.7	35.3
trans	59.5	65.8
exptl (WMS $\Delta E = 0.9$)		
gauche	27.9	24.9
trans	72.0	75.0
OPLS/MC		
gauche	30.9	24.3
trans	69.1	75.7
AMBER/MD		
gauche	31.3	23.1
trans	68.7	76.9

[a] RIS: rotational isomeric states modeling of conformational distributions correlated with the raman spectra results of Wong, Mantsch, and Snyder.[26] ΔE is the energy difference between gauche and trans energy wells in kcal/mol. OPLS/MC results are from ref 21. AMBER/MD results are from this study. Values in columns are the percentage (on average) of molecules found in the listed conformations. [b] Average of the two outer torsion angles of hexane in gauche or trans configurations, given as a percent.

Given the tolerance in matching the RIS-approximated conformational frequencies with the original Raman spectra, the AMBER/MD *n*-hexane model qualitatively reproduces the experimental conformational distribution. The conformational distribution produced by the MD simulation is most closely in agreement with the WMS RIS results generated using the 0.9 kcal/mol energy difference between trans and gauche conformations. There is excellent agreement in the ordering of conformational preferences. The triply-trans conformation (ttt) is somewhat more frequent, while the singly-gauche (gtt) conformation is slightly less frequent in the MD than in the WMS results. These two conformations (ttt and gtt) are consistently the first and second most highly preferred in all three data sets. The bottom of Table 1 reports the average percentage of gauche or trans conformations in the outer two hexane torsional rotors versus the inner rotor. The overall agreement between the WMS($\Delta E = 0.9$), OPLS/MC, and AMBER/MD is quite good.

Several other relevant studies of conformational behavior of chain molecules include the use of methods such as two-dimensional NMR (*n*-hexane)[31] and ab initio computation of normal-mode frequencies (fitting the well-assigned bands of *n*-pentane and *n*-hexane).[32] Both of these are in qualitative agreement with the results of WMS and thus also the AMBER/MD alkane model described here.

(26) Wong, P. T. T.; Mantsch, H. H.; Snyder, R. G. *J. Chem. Phys.* **1983**, *79*, 2369.
(27) Tirado Rives, J.; Jorgensen, W. L. *J. Am. Chem. Soc.* **1990**, *112*, 2773.
(28) Allen, M. P.; Tildesley, D. J. *Computer Simulation of Liquids*; Clarenden Press: Oxford, U.K., 1987; p 80.
(29) Berendsen, H. J. C.; Postma, J. P. M.; van Gunsteren, W. F.; DiNola, A.; Haak, J. R. *J. Chem. Phys.* **1984**, *81*, 3684.
(30) Cantor, C. R.; Schimmel, P. R. *Biophysical Chemistry III. The Behavior of Biological Molecules*; W. H. Freeman and Co.: New York, 1971; p 194.
(31) Gochin, M.; Pines, A.; Rosen, M. E.; Rucker, S. P.; Schmidt, C. *Mol. Phys.* **1990**, *69*, 671.
(32) Mirkin, N. G.; Krimm, S. *J. Phys. Chem.* **1993**, *97*, 13887.

Table 2. Molecular-Mechanical Interaction Parameters for Hydrocarbon, Hydroxyl, and SPC Water[a]

VDW type	R^*	ϵ	Q	description
OW	1.7765	0.155 45	−0.810	−O−, SPC water
HW	0.0000	0.000 00	0.420	−H−, SPC water
HL	0.0000	0.000 00	0.435	−H−, 1-alkanol; H−O, hydrogen
Oh	1.7230	0.170 00	−0.700	−O−, 1-alkanol; O−H, oxygen
Mo	2.1915	0.118 00	0.265	$-CH_2-$, 1-alkanol; C−O, carbon
ML	2.1915	0.118 00	0.000	$-CH_2-$, *n*-alkane chains
Me	2.1915	0.150 00	0.000	$-CH_3$, alkane end methyl

bond	R_{eq}
HL−Oh	0.945
Oh−Mo	1.430
Mo−ML	1.530
ML−ML	1.530
ML−Me	1.530
OW−HW	1.000
HW−HW	1.633

angle	FC	τ_{eq}
HL−Oh−Mo	55.000	108.500
Oh−Mo−ML	80.000	112.000
Mo−ML−ML	63.000	112.000
ML−ML−ML	63.000	112.000
ML−ML−Me	63.000	112.000
HW−OW−HW	100.000	109.470
OW−HW−HW	100.000	35.265

torsion	V_N	shift	period
HL−Oh−Mo−ML	0.40	0.000	3
HL−Oh−Mo−ML	0.36	0.000	1
Oh−Mo−ML−ML	1.42	0.000	3
Oh−Mo−ML−ML	0.08	180.000	2
Mo−ML−ML−ML	1.42	0.000	3
Mo−ML−ML−ML	0.08	180.000	2
ML−ML−ML−ML	1.42	0.000	3
ML−ML−ML−ML	0.08	180.000	2
Me−ML−ML−ML	1.42	0.000	3
Me−ML−ML−ML	0.06	180.000	2
Me−ML−ML−Me	1.42	0.000	3
Me−ML−ML−Me	0.06	180.000	2

[a] Force constants FC are in kcal/(mol/rad^2) for angles, from the Weiner et al. force field.[22] SHAKE was used for all bonds. Geometries are OPLS,[21] bond lengths R_{eq} in angstroms, angles τ_{eq} in degrees. The two-term dihedral barrier heights are as found in an AMBER input parameter file.[22] Shift is the phase shift, and period is the numerical periodicity for the torsion angle. R^* and ϵ are the radius (Å) and well depth (kcal/mol) for Lennard-Jones VDW-type nonbonded atomic interactions and Q is the partial atomic charge.

4. Hydrated 1-Octanol Systems and Liquid Modeling Details. simple point charge (SPC) waters[33] were used in the water-saturated 1-octanol model. The systems were slightly less than maximally water saturated in each case. The mole fraction of water X_{wat} in fully water-saturated octanol is temperature dependent. X_{wat} is 0.245 at 20 °C, 0.255 at 25 °C, 0.290 at 40 °C, and 0.366 at 75 °C as measured by experiment.[34] Simulations of water-saturated octanol analyzed for structural and dynamic properties were carried out at 40 °C with X_{wat} equal to 0.250 (228 octanols, 76 waters). A system containing 125 octanols and 42 SPC waters was used to evaluate thermodynamic properties at 25 °C, with X_{wat} at 0.251. The FEP simulation at 37 °C contained 98 octanols, 26 SPC waters, and one solute, giving X_{wat} equal to 0.208.

For water-saturated octanol, 76 waters from a pre-equilibrated system were surface-juxtaposed to the 228 molecule pre-equilibrated octanol system. After initial brief relaxation, the temperature was increased to 500 °C (under constant-volume conditions) until a uniform distribution of the water molecules was achieved. The temperature was then incrementally decreased to 25 °C, annealing over a period of 1.0 ns. Equilibration followed, beyond energetic and volumetric limiting values (to 2.0 ns), allowing configurational reorientation of water and octanol molecules at 25 °C prior to any data collection.

For the benzene-to-phenol perturbation, a benzene hydrogen is mutated into the hydroxyl group of phenol. Each end state was relaxed for 200 ps before beginning the bidirectional perturbation calculations, each covering a total of 2.6 ns. The aqueous (SPC water model) benzene-to-phenol perturbation was done as a 50-window FEP calculation, 100 ps (40/60 equilibrate/collect) in each of forward and reverse directions (after 20 ps end-state relaxations), at a constant temperature of 310 K, using a 10 Å residue-based nonbonded cutoff, updating the pair list each 20 MD steps. The aromatic solute is solvated in a periodic box of water-saturated octanol solvent (98 octanols, 26 SPC waters, obtained by "slicing down" and then re-equilibrating the 228:76 box), averaging approximately 30.2 Å per side. The all-atom benzene and phenol parameters were those of Jorgensen.[35] The temperature was maintained at 310 K to encourage reorientation within the octanol media. Detailed descriptions of the FEP methodology and these particular FEP calculations have been given elsewhere.[36,37]

The long hydrocarbon chains were modeled as multiple (bonded) residues. For hexane, the molecule was broken down into two residues, atoms 1−3 and 4−6, where the first atom of each residue was used to determine residue pairing. For octane, two residues of four atoms apiece were used. 1-Octanol was partitioned into four residues of atoms 1−3, 4−5, 6−7, and 8−10, where atom 1 is the hydroxyl hydrogen.

An MD step size of 2.0 fs was used for all liquid-phase calculations. All molecular bonds were constrained to their equilibrium lengths with holonomic constraints via SHAKE, within a tolerance of 0.0001 Å or finer. Simulations were carried out with periodic boundary conditions, at constant pressure (1 bar) and temperature, with separate temperature coupling for the solute and solvent. Spherical residue-based nonbonded interaction cutoffs of 9 Å (hexane, octane) or 10 Å (1-octanol) were used. Temperature was coupled to a heat bath with a relaxation time τ_T of 0.2 ps. The pressure coupling τ_P was also set to 0.2 ps. Nonbonded pair lists were updated every 30 MD steps for simulations involving octanol.

Reaction field conditions, a long-range electrostatic modeling methodology,[38] was implemented within AMBER's MD module, so that simulated liquid 1-octanol qualitatively mimics the dielectric traits of the macroscopic medium (details provided in later section). For the calculation of bulk dielectric fluctuations the three-dimensional $\mathbf{M}(t)$ was computed at every MD step. Coordinates of the system(s) were saved every 0.1 or 0.05 ps for structural and dynamic analyses.

5. Reproduction of Physical and Thermodynamic Properties. The computed physical properties of the MD-modeled pure liquids hexane, octane, and 1-octanol are reported in Table 3 along with the experimentally measured values. Jorgensen's OPLS/MC results for hexane[21] are restated in Table 3 for comparison. Note that densities (in terms of volume per molecule) and molar enthalpies of vaporization from MD simulations are all in acceptable agreement with experimentally determined physical properties (percent deviations are given in parentheses in Table 3). No long-range van der Waals correction was added in these simulations. On the basis of other MD simulations[39] of water, methanol, and *N*-methylacetamide, these corrections can increase the ΔH_{vap} and decrease the molar volume in the range 0−5%.

The density of water-saturated octanol can be calculated using the known value for the partial molar volume of water added to octanol. The volume of water at 298 K is slightly less at saturation levels in

(33) Berendsen, H. J. C.; Postma, J. P. M.; van Gunsteren, W.; Hermans, J. In *Intermolecular Forces*; Pullman, B., Ed.; Reidel: Dordrecht, The Netherlands, 1981; pp 331−342.
(34) von Erichsen, L. *Brennst.−Chem.* **1952**, *33*, 166−172.
(35) Jorgensen, W. L.; Nguyen, T. B. *J. Comput. Chem.* **1993**, *14*, 195.
(36) DeBolt, S. E.; Pearlman, D. A.; Kollman, P. A. *J. Comput. Chem.* **1994**, *15*, 351.
(37) Beveridge, D. L.; Di Capua, F. M. *Annu. Rev. Biophys. Biophys. Chem.* **1989**, *18*, 431. Pearlman, D. A.; Kollman, P. A. *J. Chem. Phys.* **1989**, *90*, 2460. van Gunsteren, W. F. (pp 27−59) and Pearlman, D. A.; Kollman, P. A. (pp 101−119) in: van Gunsteren, W. F.; Weiner, P. K. *Computer Simulations of Biomolecular Systems: Theoretical and Experimental Applications*; ESCOM: Luden, The Netherlands, 1989. Singh, U. C.; Brown, F. K.; Bash, P. A.; Kollman, P. A. *J. Am. Chem. Soc.* **1987**, *109*, 1607−1614.
(38) Allen, M. P.; Tildesley, D. J. *Computer Simulation of Liquids*; Clarendon Press: Oxford, U.K., 1987; Chapter 5, p 162.
(39) Caldwell, J. W.; Kollman, P. A. *J. Phys. Chem.*, in press.

Table 3. Physical Properties of Pure Liquids[a]

	ΔH_{vap}	volume/molecule
	Hexane	
expt[b]	7.54	218.5
OPLS/MC[c]	8.07 (7.0%)	211.5 (3.3%)
AMBER/MD[d]	7.25 (3.8%)	215.9 (1.2%)
	Octane	
expt[b]	9.91	272.1
AMBER/MD	9.72 (1.9%)	273.9 (0.7%)
	Octanol	
expt[b]	15.60	262.8
AMBER/MD	16.39 (5.0%)	265.2 (0.9%)

[a] Heat of vaporization ΔH_{vap} and volume per molecule data from simulations of 125 (hexane and octane) or 250 (octanol) molecules (volume in Å^3, ΔH_{vap} in kcal/mol). The percent deviation of computed values from experimentally determined values are given in parentheses. The standard deviations for computed values are less than 1.0 Å^3 for volumes and slightly less than 0.1 kcal/mol for ΔH_{vap} values. The temperature was 298 K for all simulations and for experimental values. Results are after averaging over several MD liquid simulations summing from 300−1000 ps after extensive system relaxation and 2.0−4.0 ns for individual gas-phase molecule MD simulations (details in text). [b] Selected values of Properties of Chemical Compounds, Manufacturing Chemist's Assn. (*Phys. Chem. Rev. Data* **1973**, 2). [c] As per Monte Carlo simulations using OPLS parameters by W. L. Jorgensen in ref 21. [d] AMBER/MD nonbonded interaction parameters as per Table 1, scaled by 1/7.4 for intramolecular 1−4 contacts, using 9.0 Å (hexane and octane) or 10.0 Å (octanol) spherical nonbonded cutoff.

octanol (17.92 cm^3 mol^{-1}) than in pure water (18.57 cm^3 mol^{-1}).[40] This produces a slight contraction of volume in the octanol/water media relative to what would be observed if pure octanol and pure water were simply volume additive. For the water-saturated octanol system containing 125 octanols and 42 waters, the experimental volume at 25 °C is 34 100 Å^3/system, arrived at by using the experimental volume per molecule for octanol (262.8 Å^3) and for saturation waters (29.76 Å). Simple volume additivity would result in 34 145 Å^3. The AMBER/MD model closely reproduced the correct binary system density, 34 014 Å^3/system, differing from the experimental value by only 0.25%. The standard deviation associated with the MD-computed value is ±402, due to normal volume fluctuations over the 1.0 ns MD averaging period.

The heat of vaporization of water-saturated octanol was not available for comparison. As a rough approximation, the heat of solution of water vapor in pure 1-octanol at infinite dilution is given as 9.72 kcal/mol by subtracting the heat of solution of liquid water in 1-octanol at infinite dilution (0.80 kcal/mol) from the heat of vaporization of liquid water at 25 °C (10.52 kcal/mol).[41] Because experimental heats of dilution are generally sensitive to concentration, this approximation for the heat of solution is not strictly rigorous. The computed ΔH_{vap} from the MD simulation is 2049 ± 20 kcal for a 125-molecule pure octanol system (by multiplying the molar ΔH_{vap} given in Table 3 for pure octanol by 125) and 2516 ± 36 for the mixed 125/42 octanol/water system. Waters therefore contribute 442 kcal, or about 10.5 kcal/mol, to ΔH_{vap} for modeled water-saturated 1-octanol. The computed number, 10.5, is within 8% of the experimental (infinite dilution) number, 9.72. In addition, this was *not* a simulation of the solvation of an isolated water (infinite dilution) in pure octanol, where each of the water molecule's first-solvent-shell hydrogen-bonding sites would be occupied only by octanol molecules. One should expect a water molecule to be more strongly bound in *water-saturated* octanol than at infinite dilution, stronger in proportion to the number of first-shell sites that are occupied by other waters of saturation rather than by octanol molecules. For comparison, SPC-modeled pure water also has a potential energy value of about 10.5 kcal/mol,[33] suggesting that saturation waters may be nearly as tightly bound in hydrated 1-octanol as in pure water. By following this rationale, it is likely that the computed value of 10.5 kcal/mol is reproducing within *closer* than 8% the true heat of solution of an isolated water in *water-saturated* octanol.

Overall, simulations employing these AMBER/MD long-chain alkanol parameters have reproduced critical thermodynamic and physical liquid properties. This provides an excellent model system for studying the structure and dynamics of octanol media as well as for use in solvation studies.

B. Background Material Regarding Dielectric Phenomena. The macroscopic static dielectric constant ϵ_0, or zero frequency relative permittivity, is a measure of a substance's ability to act as an electrical insulator. In the absence of an external field, liquid molecules undergo chaotic motion; the bulk dipole moment $\langle \mathbf{M} \rangle_{time} = \langle \Sigma_i \mu_i \rangle_{time}$, taken over all molecular dipoles, equals zero. Imposition of a static electrical field $\mathbf{E}_0$ promotes the directional alignment of all polar and polarizable groups in the media, giving rise to collective reorientation. This produces a net polarization, $\langle \mathbf{M} \rangle_{time} \neq 0$, counter to the applied field. This dielectric response occurs as a time-dependent dynamic process during which molecular rearrangements occur until an equilibrium-induced field condition is reached. Using microwave spectroscopy, the process of depolarization is measured as the exponential decay with time of the polarization in a dielectric when the externally applied field is removed. This is usually expressed as a relaxation time $\tau_r = 1/k_{rate}$. Even in the absence of external fields, a local region of the dielectric media may temporarily attain a polarized condition $\mathbf{M}_{local} \neq 0$ as it responds to fleeting electrical perturbations created by the chaotic motions in the surrounding media. Spontaneous fluctuations (bulk or local) in $\mathbf{M}$ average to zero over time, i.e. $\langle \delta \mathbf{M}(t) \rangle_{time} = 0$.

The orientational polarization resulting from the rotational alignment of polar molecules and rotatable polar groups is the most substantial contributor to ϵ_0. The strongest polar group in 1-octanol is the H−O−C alkoxyl "head group". The gas-phase dipole for this group is about 1.7 D. In comparison, water has a dipole of about 1.85 D in the gas phase. The liquid-phase "apparent" dipole of the 1-octanol molecule is 2.88 D (20 °C). A range from 2.35 to 2.82 D is generally accepted for liquid water.[42-45] The weak permanent bond dipoles of the H−C bonds of the hydrocarbon are considered as "averaged to zero" in this model.

Another minor contribution to ϵ_0 results from the distortional polarization that arises from the stretching and bending of bonds connecting polar atoms. This contribution is partially accounted for by the angle bending included in the molecular model. An electronic (or atomic) polarization response occurs even in the presence of a very high frequency oscillating field, giving rise to the optical dielectric constant ϵ_∞. In this study, no explicit electronic polarizability is simulated; the contribution of electronically polarizable groups to the bulk static dielectric constant ϵ_0 is ignored. At very high frequencies the relative permittivity of 1-octanol is about $\epsilon_\infty = 2.15$.[46]

1-Octanol has three dispersion regions and thus three internal dielectric response mechanisms; one occurring (data at 20 °C) at (1−22) × 10^{10} s^{-1} is the major contributor, and those at (1.7−5) × 10^{11} and (1.4−4) × 10^{12} s^{-1} are lesser contributors.[46] The frequency-dependent dielectric value $\epsilon(\omega)$ reflects how rapidly the media can reorient its set of dipole vectors (its bulk moment) with respect to an externally imposed oscillating electrical field.

Each dielectric response mechanism corresponds to a dynamic molecular motion and exhibits a characteristic decay or relaxation time, τ_r. Fortunately, it is possible to calculate these τ_r, via MD simulations, without simulating an explicitly applied electrical field. The τ_r values are determined by examining the time correlation of the spontaneous fluctuations, $\delta \mathbf{M}$, at equilibrium in the absence of an external field. The fluctuation−dissipation theorem states, "In a system close to equilibrium, we cannot distinguish between spontaneous fluctuations and deviations from equilibrium that are externally prepared".[47] This means that the relaxation of a macroscopic nonequilibrium disturbance (such as the displacement from equilibrium by application of a field) is governed by the same laws and exhibits the same decay characteristics as the regression of spontaneous fluctuations in an equilibrium system. Thus, the rate of decay of a macroscopic nonequilibrium process (such

(40) Berti, P.; Cabani, S.; Mollica, V. *Fluid Phase Equilib.* **1987**, *32*, 195−203.
(41) Marcus, Y. *J. Solut. Chem.* **1990**, *19*, 507.
(42) Anderson, J.; Ullo, J. J.; Yip, S. *J. Chem. Phys.* **1987**, *87*, 1726.
(43) Neuman, M. *J. Chem. Phys.* **1985**, *82*, 5663.
(44) Eisenberg, D.; Kauzmann, W. *The Structure and Properties of Water*; Clarendon Press: Oxford, U.K., 1969; pp 189−94. Pople, J. A. *Proc. R. Soc. A* **1951**, *205*, 163.
(45) Onsager, L. *J. Am. Chem. Soc.* **1936**, *58*, 1486, eq 30. Oster, G.; Kirkwood, J. G. *J. Chem. Phys.* **1943**, *11*, 175.
(46) Garg, S. K.; Smyth, C. P. *J. Phys. Chem.* **1965**, *69*, 1294.
(47) Chandler, D. *Introduction to Modern Statistical Mechanics*; Oxford University Press: New York, 1987; Chapter 8, p 241.

as the depolarization that occurs on removal of an electrical field) may be calculated from the correlation of spontaneous fluctuations of an associated microscopic observable ($\delta\mathbf{M}(t)$ in this case) in an equilibrium system.

1. Computing the Static Dielectric Using an MD Ensemble. Frohlich expressed Onsager[45] and Kirkwood's[45,48] theory of orientational polarization in terms of statistical mechanical relations involving dipole-moment fluctuations due to the changing position vectors of the charges in time.[49] Frohlich obtained this generalization of Kirkwood's extension of Onsager's equation:

$$\frac{4\pi}{3}\frac{\langle\mathbf{M}^2\rangle}{3Vk_BT}=\frac{\epsilon_0-\epsilon_\infty}{\epsilon_0+\epsilon_\infty}\left[1-\frac{(\epsilon_0-\epsilon_\infty)(\epsilon_{RF}-1)}{(\epsilon_0+\epsilon_\infty)(\epsilon_{RF}+1)}\right]^{-1} \quad (3)$$

where V represents the volume of dielectric, k_B is the Boltzman constant, T is the temperature, and $\langle\mathbf{M}^2\rangle$ is equal to $\langle\Sigma_{ij}\mu_i\cdot\mu_j\rangle$, accounting for the interaction of molecular dipoles. The reaction field fluctuation term for handling long-range electrostatic interactions has been included here in square brackets; ϵ_{RF} is the dielectric of a continuum surrounding the central sphere of explicitly modeled molecular media. The Kirkwood–Frohlich relations, coupled with an explicit consideration of surrounding media effects (via the reaction field model in this case) can be implemented within a molecular dynamics regime.[50,51] Several different boundary conditions may be used. When the system is immersed in a continuum with $\epsilon_{RF}=\infty$, an infinitely conducting dielectric, substituting ∞ for ϵ_{RF} in eq 3, and rearranging to solve for ϵ_0, gives

$$\epsilon_0=\epsilon_\infty+\frac{4\pi\epsilon_\infty\langle\mathbf{M}^2\rangle}{3Vk_BT} \quad (4)$$

A value of $\epsilon_\infty = 1.0$ (for an electronically nonpolarizable media) is used when distortional and electronic polarization effects are not explicitly treated in the simulation.[49–53]

The reaction field method[38,45] was employed to treat long-range electrostatics. The field on a dipole in the simulation consists of two parts, a short-range contribution for the explicit molecules situated within the interaction cutoff sphere and a long-range contribution arising from implicit molecules surrounding the interaction sphere. These implicit molecules are considered to form a dielectric continuum with dielectric constant ϵ_{RF}. When the continuum is polarized by the molecules within the cavity, it in turn produces a polarization response within the cavity. The interaction between these two regions approximates the dielectric friction which would exist between local regions in a macroscopic media. Neumann showed that it is not possible to accurately compute a dielectric constant via MD if this long-range effect is ignored.[54] The following term[38] is added to the molecular mechanical potential energy equation[36] to correct for the additional torques arising in the presence of a reaction field:

$$\nu_{RF}=\frac{2(\epsilon_{RF}-1)}{2\epsilon_{RF}+1}\frac{1}{r_c^3}\sum_{a,b}^{\text{sphere}}\mu_a\cdot\mu_b=\frac{(\epsilon_{RF}-1)}{2\epsilon_{RF}+1}\sum_{i,j}^{\text{sphere}}\frac{q_iq_j}{r_c^3}r_{ij}^2 \quad (5)$$

where ϵ_{RF} is the frequency-independent dielectric constant of the background continuum, r_c is the spherical cutoff radius, and μ_a and μ_b are interacting molecular dipoles. In the site–site form of the equation, q is the atomic partial charge and r_{ij} is the distance between atoms i and j.

Using the above formulations, it is straightforward to calculate octanol's static dielectric constant, ϵ_0, from the mean square of the bulk moment by sampling thoroughly over all possible configurations. Molecular dynamics followed over a sufficient time trajectory are used to generate a representative sample of accessible states.

2. Computing the Frequency-Dependent Dielectric Relaxation. There is also a straightforward method to calculate 1-octanol's frequency-dependent relaxation time(s) τ_r. Because of the fluctuation–dissipation theorem, the dielectric relaxation time(s) τ_r can be determined by fitting the decay of the time autocorrelation $C(\delta\mathbf{M}(t))$ of the spontaneous fluctuations of the bulk moment $\mathbf{M}(t)$ to an exponential function.

$$C(\delta\mathbf{M}(t))=\frac{\langle\delta\mathbf{M}(0)\cdot\delta\mathbf{M}(t)\rangle}{\langle\delta\mathbf{M}^2\rangle}=\sum_{r=1}^{N_r}A_re^{-(t/\tau_r)} \quad (6)$$

Liquids which are Debye-like in their dielectric relaxation behavior follow an exponential decay in their depolarization; 1-octanol has been shown to be Debye-like.[46] One value of $\mathbf{M}$ was saved at every MD time step as the vector components M_X, M_Y, and M_Z.

III. Internal Structure of Pure and Water-Saturated 1-Octanol

MD simulations establish that the internal structure of liquid 1-octanol media divides naturally into four levels of structural classification. Structural features at the levels of individual *molecules*, molecular *aggregates*, and *regions* of special character will be discussed. The static dielectric constant, a macroscopic property which can be viewed as an average of *system-wide* microscopic interactions, has been computed from the MD trajectory and will be discussed in a later section along with frequency-dependent dielectric behavior.

A. Features of Individual Molecules. Features of interest at the individual-molecule level include conformational distributions and hydrogen-bonding characteristics. The orientational character of hydrogen bonds, their numbers, and types of bonding arrangements with direct neighbors are examined and compared with available experimental data. Table 4 reports the computed percentage of gauche/trans (g/t) conformations for each of 1-octanol's seven torsion angles and the distribution of the specific g/t combinations for all possible conformers in the alkyl portion of the (modeled) liquid-phase molecules. The working definitions for gauche and trans conformations are 0 to 120° g^+, 0 to −120° g^-, and 120 to 240° t. Although there is a 52% gauche/48% trans distribution for the H–O–C–C torsion, the trans conformation is slightly more populated than either the g^+ or g^- conformation considered individually. The O–C–C–C torsion (45% g, 55% t) exhibits a net trans preference but with significant gauche occupancies. The alkyl portion (24% g, 76% t) shows a strong preference for the more extended trans conformations.

The lower portion of Table 4 reports the average occupation frequencies for all possible conformational states in the eight-carbon alkyl chain portion of the liquid octanol molecules. These alkyl conformations read left to right, from torsions involving the alkoxyl methylene to those involving the tail-end methyl, i.e. gxxxt means the torsion containing the hydroxyl methylene is gauche and the torsion containing the tail-end methyl is trans. Clearly, the most preferred single conformation is when five torsions simultaneously assume the fully extended all-trans configuration, accounting for 22.1% of all chains. There are about twice as many, 43.8%, singly-gauche chains. The gauche torsion is distributed fairly evenly among the five possible positions, although a gauche torsion involving the larger tail-end methyl group is the least preferred of this group. The doubly-gauche conformations account for 27.9% of chains, with tandem gauche torsions understandably contributing the least (because of van der Waals repulsions incurred from steric contact). Triply-gauche conformations contribute only 5.9% to the total, again with triply tandem conformations occupied least frequently. Only 0.4% of the chains are quadruply-gauche, and

(48) Kirkwood, J. G. *J. Chem. Phys.* **1939**, *7*, 911–919.
(49) Frolich, H. *Trans. Faraday Soc.* **1948**, *44*, 238–44. Frolich, H. *Theory of Dielectrics*; Clarendon Press: Oxford, U.K., 1958.
(50) Neumann, M. *Mol. Phys.* **1983**, *50*, 841.
(51) Neumann, M.; Steinhauser, O. *Chem. Phys. Lett.* **1983**, *102*, 508.
(52) Scaife, B. K. P. *Principles of Dielectrics*; Clarendon Press: Oxford, U.K., 1989; p 203.
(53) Steinhauser, O. *Ber. Bunsen-Ges. Phys. Chem.* **1983**, *87*, 128–142.
(54) Neumann, M.; Steinhauser, O.; Pawley, G. S. *Mol. Phys.* **1984**, *52*, 97–113.

Table 4. Torsion Angle Distributions in (Modeled) Pure Liquid 1-Octanol[a]

torsion	%gauche	%trans
(1) HOCC	51.9	48.1
(2) OCCC	45.0	55.0
(3) CCCC	23.8	76.2
(4) CCCC	25.3	74.7
(5) CCCC	22.6	77.4
(6) CCCC	23.8	76.2
(7) CCCC	23.3	76.7
alkyl av	23.7	76.3

conformer	%	std dev	%sum
all trans:			22.1
ttttt	22.1	2.0	
one gauche			43.8
tttgt	10.5	1.5	
ttgtt	10.0	1.3	
tgttt	8.3	1.4	
gttt	7.9	1.2	
ttttg	7.1	1.2	
two gauche			27.9
gttgt	4.4	0.8	
ttgtg	3.9	0.9	
tgtgt	3.7	0.9	
ttggt	3.5	0.8	
tgttg	3.4	0.9	
gtgtt	3.2	0.9	
gtttg	1.6	0.9	
tggtt	1.6	0.6	
ggttt	1.5	0.7	
tttgg	1.1	0.6	
three gauche			5.9
gtgtg	1.2	0.7	
gttgg	0.8	0.5	
ggtgt	0.7	0.4	
ggttg	0.6	0.4	
gggtt	0.6	0.4	
ttggg	0.6	0.4	
tgtgg	0.4	0.3	
tgggt	0.4	0.3	
tggtg	0.3	0.2	
gtggt	0.3	0.2	
four gauche			0.4
tgggg	0.1	0.1	
gggtg	0.1	0.4	
ggtgg	0.1	0.2	
ggggt	0.1	0.1	
gtggg	0.03	0.1	
all gauche			0.0
ggggg	0.00	0.0	

[a] Averages taken over 1285 coordinate sets of 250 molecules, 0.1 ps apart, at 25 °C.

in a sample of 321 250, no quintuply-gauche chains were found. The results of a previous MD simulation of *n*-octane[55] are comparably similar (having the same ranking but nonidentical percentages) to those presented in Table 4 for 1-octanol conformational preferences.

B. Hydrogen-Bonded Aggregates. The typical environment of an octanol hydroxyl group and its orientation relative to its nearest solvent shell neighbors can be determined by referring to its radial pair distribution function (RDF)[38] as in Figure 1. A working definition for a hydrogen bond was chosen as any two hydroxyl oxygens closer than 3.5 Å, having one of their hydrogens contained between, where the angle of $O'^{H}\cdots O$ is no greater than 30° at the maximum O−O distance. As the RDF's g(O,O) (solid line) and g(O,H) (broken line) indicate, most O−O and O−H hydrogen-bond distances are well inside these geometric limiting criteria. On average, an octanol oxygen O_c "sees" two other oxygens about 2.75 Å away, one hydrogen

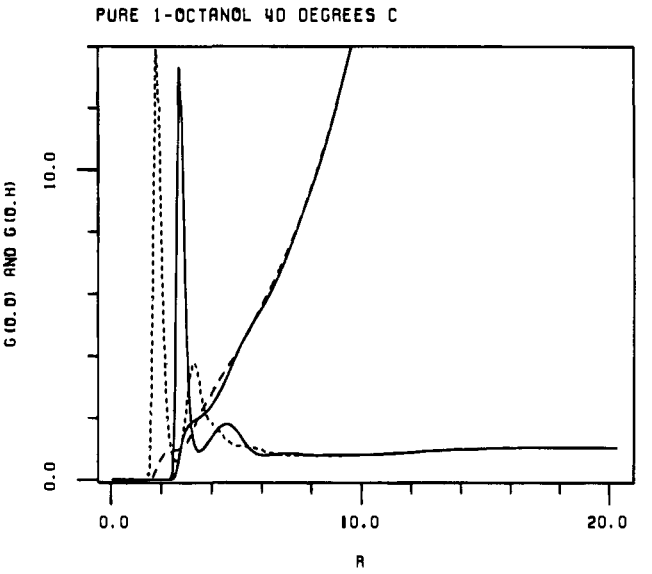

Figure 1. Radial pair distribution functions in pure 1-octanol. Plots are g(O,O) between hydroxyl oxygens (solid line) and g(O,H) between the oxygen and surrounding hydroxyl hydrogens (broken line). Integrating the RDFs gives the coordination numbers c(O,O) (solid line) and c(O,H) (broken line). Long dash line at $g = 1$ from $R = 0$ to $R = 20$ Å is for reference. Data from averaging 250 molecules of pure 1-octanol at 40 °C, over more than 30 000 coordinate sets, about 2 ns MD.

at 1.9 Å and a second hydrogen about 3.25 Å away (see the integration line data between 0.0 and 3.5 Å for the coordination numbers). Octanol oxygen O_c is hydrogen bonded to two other oxygens; one (with its attached hydrogen at $R = 1.9$ Å) is a donor to O_c, and the other (with its hydrogen at $R = 3.25$) is an acceptor of O_c's hydrogen. By the law of cosines, the average angle $O'^{H}\cdots O_c$ between the donating neighbor and O_c is 21°, putting the hydrogen out of plane so the bond is not strictly linear. Some "bending" of hydrogen-bonding polymer chains may influence this. As a reference for comparison, the analogous angle between water dimers has been experimentally measured as $6 \pm 10°$.[56] The average angle $O_c\cdots O'^{H}$ between O_c and the accepting neighbor is 114°. There are two more hydroxyl oxygens within 5.0 Å of O_c as evidenced by the second peak at about $R = 4.5$ Å and the coordination plot. A very low third peak appears at $R = 7.0$ Å. It is apparent that hydroxyl oxygen O_c is (on average) a member in a chain of hydrogen-bonded molecules or some other complex of hydroxyl groups.

It is well established that some form of polymeric hydrogen-bond-linked aggregate is present in alcohols and their solutions.[57-62] Several possible hydrogen-bonded polymeric species have been hypothesized, but no definitive description has been given, leaving many unanswered questions. Are there long polymeric chains, or closed ring structures, or both? Are there various sizes and configurations, or are there a limited number of species? Is there a rapid turnover of such structures? What is the influence of temperature on the internal structure and dynamics of the media?

This MD study finds that 1-octanol forms variable-sized hydrogen-bond-linked aggregates or "clusters". A cluster

(55) Hammonds, K. D.; McDonald, I. R. *Chem. Phys. Lett.* **1993**, *213*, 27.

(56) Dyke, T. R.; Mack, K. M.; Muenter, J. S. *J. Chem. Phys.* **1977**, *66*, 498.

(57) Grunwald, E.; Pan, K. C. *J. Phys. Chem.* **1976**, *80*, 2929.

(58) Fletcher, A. N.; Heller, C. A. *J. Phys. Chem.* **1967**, *71*, 3742.

(59) Iwahashi, M.; Hayashi, Y.; Hachiya, N.; Matsuzawa, H.; Kabayashi, A. *J. Chem. Soc., Faraday Trans.* **1993**, *89*, 707.

(60) Dannhauser, W. *J. Chem. Phys.* **1968**, *48*, 1918.

(61) Shinomiya, T. *Bull. Chem. Soc. Jpn.* **1989**, *62*, 3643, 2258.

(62) Karachewski, A. M.; Howell, W. J.; Eckert, C. A. *AIChE J.* **1991**, *37*, 65. Karachewski, A. M.; McNiel, M. M.; Eckert, C. A. *Ind. Eng. Chem. Res.* **1989**, *28*, 315.

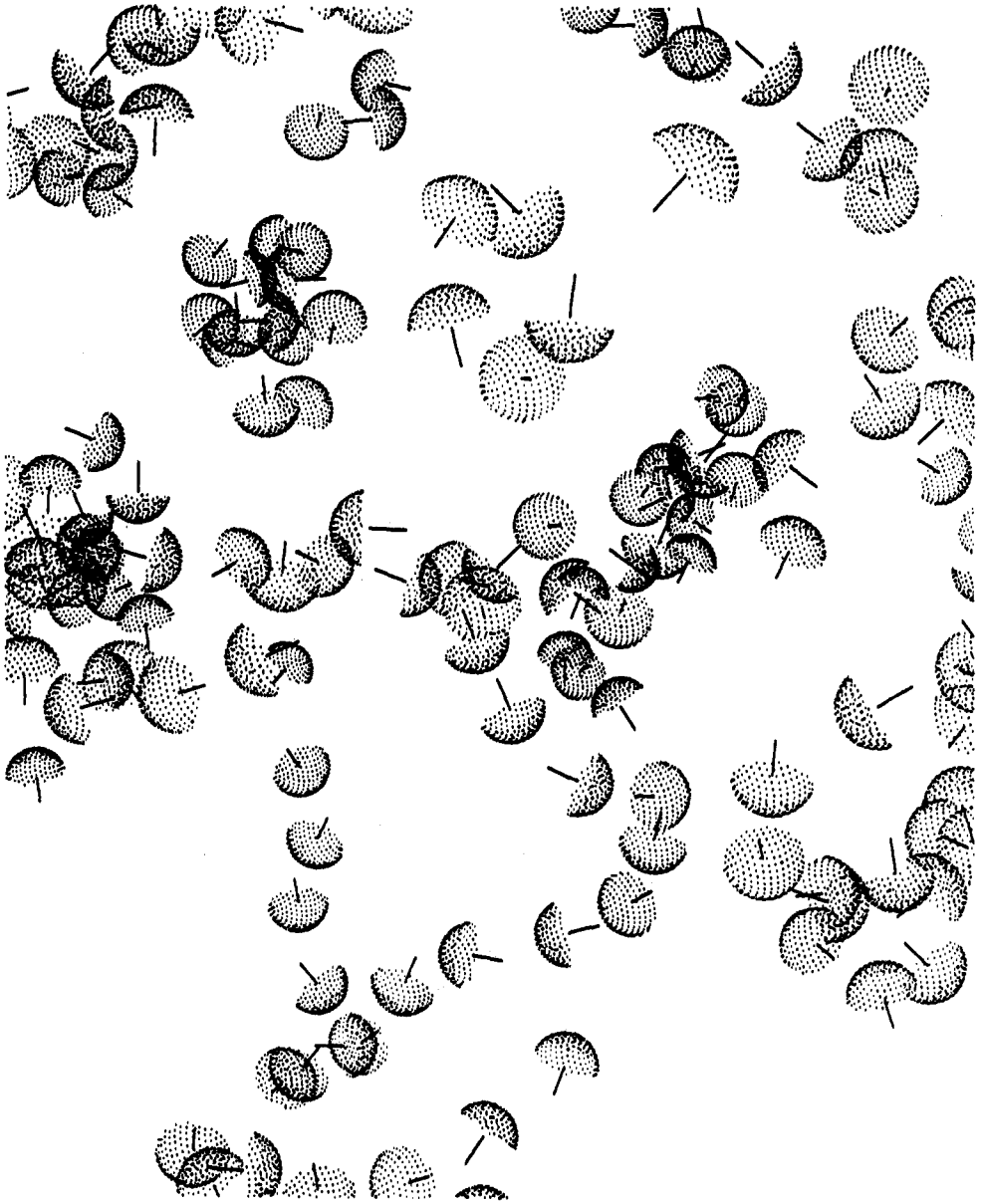

Figure 2. Hydrogen-bonded "hydroxyl polymers" in pure 1-octanol. The dot-surface hemispheres represent one-half the van der Waals radius of a hydroxyl hydrogen. The straight lines represent the bond vector from the hydrogen to the hydroxyl oxygen. The direction of hydrogen bonding is clear. Depending on the 3-D orientation of this sample, many chains and ring structures can be distinguished. Note the 5-membered ring in the upper-central region.

structure is identified by choosing an initial molecule, designating any molecules hydrogen bonding to it, then continuing to follow along the chain(s) of hydrogen-bond connectivity until there are no more. As described above, the great majority of molecules serve as donor−acceptor links in a hydrogen-bonded network. Figure 2 is a snapshot from a pure 1-octanol MD trajectory, a typical configuration, emphasizing the orientations of hydroxyl groups. The tendency for molecules to form polymeric networks of hydrogen bonds is equivalent. But while long chains can be seen coursing through the media, alongside are smaller closed-loop ring clusters and some more densely packed aggregates as well. All of these structural features are present simultaneously in this structurally heterogeneous media.

Table 5 reports the numbers, types, and percentages of hydrogen-bond "types" formed at two temperatures in pure 1-octanol. The values in the upper section of Table 5 are the actual *numbers* of items found on average in a periodic system of 250 molecules. In the lower section, the values are recast as the *percentage* of all 250 molecules which appear as a particular given species. There are fewer clusters found per coordinate set (24.1 versus 32.5) at 40 °C than at 75 °C, reflecting the greater number of molecules per cluster (10.4 versus 7.4) at the lower versus higher temperature. The division of this data into rings per set and chains per set indicates that an overall preference for rings versus chains is reversed as temperature increases, as expected based on the influence of entropy. There is a marked increase in the number of monomers at higher temperature. It was important to establish the number of unpaired hydroxyl hydrogens, referred to as nondonors in Table 5, as this provides a comparison against available near-infrared data. Acceptor-only molecules are those whose oxygen acts as a hydrogen-bond acceptor but whose hydroxyl hydrogen is unbound. Nondonors are the number of acceptor-only plus the number of monomers. Donor-only molecules are those whose hydrogen acts as a hydrogen-bond donor but whose hydroxyl oxygen is unbound. Nonacceptors are the number of donor-only plus monomers. The number of partially-unbound species increases with temperature as rings are broken and large clusters break down. The percentage of free (unbound) hydroxyl hydrogens calculated from the MD simulation can be compared with the experimental near-infrared results of Grunwald and Pan (GP).[57] GP determined the mole fraction of free hydroxyl

Table 5. Pure Liquid 1-Octanol Hydrogen Bonding and Cluster Analysis in a 250 Molecule Box[a]

av quantities	40 °C	75 °C
clusters per set	24.1	32.5
molecs per cluster	10.4	7.4
rings per set	16.6	15.7
chains per set	9.2	18.4
monomers per set	4.5	11.9
nondonors (free H)	13.0	27.8
acceptor-only	8.5	15.9
nonacceptors (free O)	25.9	40.0
donor-only	21.4	28.1
species	**% @ 40 °C**	**% @ 75 °C**
monomers	1.8	4.8
donor-only	8.6	11.2
free OH oxygen	10.4	16.0
acceptor-only	3.4	6.4
free OH hydrogen	5.2	11.1
free OH hyd expt[b]	5.4	11.2

[a] Averages taken over 62 400 (40 °C) or 78 000 (75 °C) coordinate sets, each set composed of 250 molecules. Notice that the number of clusters multiplied by the number of molecules per cluster, plus the number of monomers, gives approximately 250, the number of molecules in the simulation. Also note that the number of rings plus chains plus monomers does not exactly equal the average number of clusters. Discrepancies are due to the formation of multiple rings within some large clusters and rounding within the analysis program. [b] Experimental numbers from Grunwald and Pan.[57]

hydrogens from the sharp band intensity at 1430 nm, which signals the first overtone region of the free OH bond-stretching vibration. A broad band spanning from about 1430 to beyond 1700 nm represents OH stretching when the hydroxyl hydrogen is hydrogen bonded; GP attribute this to some generic polymeric species. For MD simulations we have designated the species causing these two stretching regions as (1) the nondonors and (2) those which participate in ring clusters or polymeric chains by at least donating. There is very close agreement between experimental[57] and MD results regarding the percentage of free hydroxyl hydrogens present on average (see Table 5, lower section). The 40 °C MD simulation predicts 5.2% of hydroxyl hydrogens are unbound; the experimentally determined value is 5.4%. The 75 °C MD simulation predicts 11.1% of hydroxyl hydrogens are unbound; the experimentally determined value is 11.2%. This indicates the degree of realism in the model's representation of 1-octanol's internal hydrogen bonding and lends credibility to further observations made here regarding the structural specifics of hydrogen-bonded species and cluster-size distributions.

In Figures 3 and 4, the histograms illustrate the frequency distribution of cluster sizes from MD simulations of pure 1-octanol at 40 and 75 °C, respectively. The main display histograms report the percent of molecules (y-axis) which participate in a cluster of a given size (x-axis). The inset histograms report the actual number of clusters (y-axis) of a given size (x-axis) that were present on average in a system of 250 molecules. Although there is a significant occurrence frequency of very large sized aggregates, note the tendency to preferentially form four-, five-, and six-membered clusters (and seven-membered at 40 °C) and the conspicuous unfavorability of two- and three-membered complexes. It should not be surprising that pentagonal and hexagonal motifs are present;

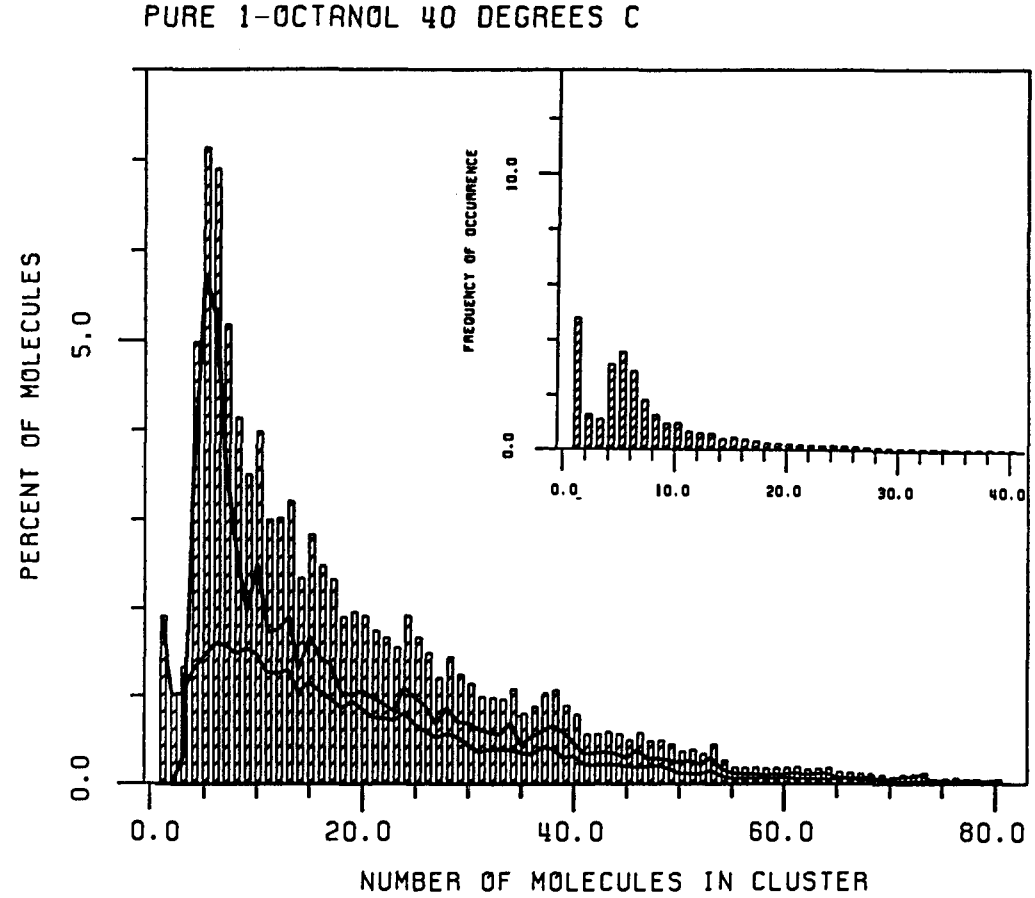

Figure 3. Frequency distribution of pure 1-octanol clusters of various sizes at 40 °C. The main display reports the percent of molecules which participate in a cluster of a given size. The inset reports the actual number of clusters of a given size found in a periodic box of 250 molecules. The uppermost solid line drawn through the histogram indicates the contribution from species containing rings; the lowermost solid line indicates the contribution from open-chain species. Data collected as in Table 5.

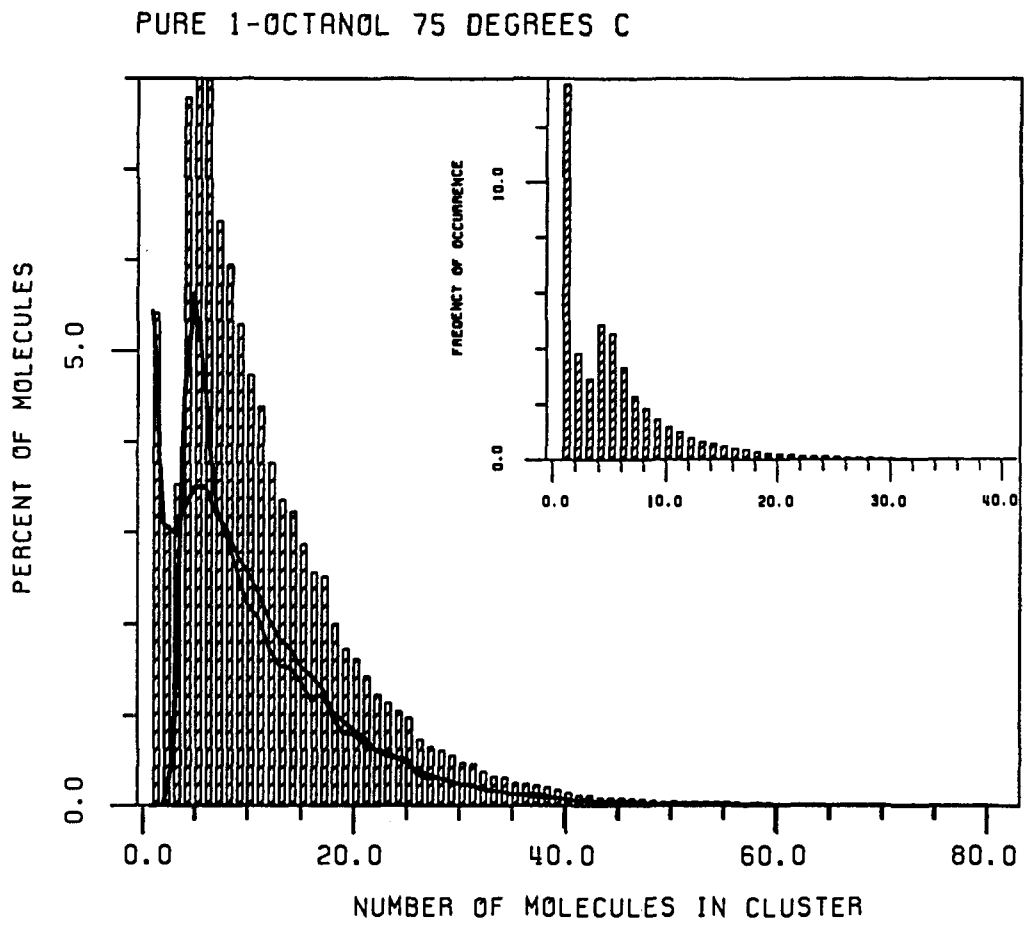

Figure 4. Frequency distribution of pure 1-octanol clusters of various sizes at 75 °C, otherwise as in Figure 3.

these are also prevalent in ice water,[63] where the hydrogen bonds are more linear and energies are optimized. The factor of finite system size is probably not significantly influencing the distribution since the strongly preferred cluster size is very small relative to the overall number of molecules.

In hydrogen-bonded complexes that form linear open-ended chains, each chain has one "uncompleted" hydrogen bond as a result of the free oxygen acceptor and hydrogen donor on opposite ends of the chain. The shorter a chain is, the lower is the ratio N_B/N_M of the number of hydrogen bonds formed (N_B) relative to the number of molecules involved (N_M), i.e. 0/1 for monomers, 1/2 for dimers, 2/3 for trimers, 3/4 for a tetramer, and so forth. As the size of a chain increases, the N_B/N_M ratio increases, optimizing the average enthalpy gained per molecule involved in an aggregate, causing larger aggregates to be more stable. But why are dimers and trimers so relatively unstable, and why the sudden increased stability in going from a trimer to a tetramer?

When a four-membered hydroxyl chain bonds back onto its own terminus, closing to form a polymeric ring, N_B/N_M becomes 4/4 rather than 3/4. Ring structures of any size should be enthalpically favored. Another way to increase the ratio would be in forming more than two hydrogen bonds per hydroxyl group, giving rise to branching and the possibility of multicyclic rings. There may be enough extra strain in forming cyclic trimers to overshadow much of the gain. Their H···O$'^{H}$ angles must be nearly 60° to form linear hydrogen bonds, far from the more optimal 110–120° (because of the lone pair geometry). In a cyclic trimer, all three partially positively charged hydroxyl hydrogens are very proximally located, causing electrostatic repulsion. In the case of a dimer, a true cyclic ring cannot be formed, although bifurcated hydrogen bonds may be possible, subject to strain akin to that in the trimer.

If higher order aggregates are preferable from an enthalpic standpoint, why is there a clear trend of decreasing frequency as N_M grows beyond five or six? In fact, a single massive inter-hydrogen-bonded network involving all molecules in the system does form, but with very low frequency, likely due to the decrease in entropy as aggregate size increases. With an increase in temperature, the entropy factor should contribute an increase in the free energy of the higher order aggregates, likely decreasing their frequency even more. In comparing Figures 3 and 4, a decrease in the number of larger aggregates at higher temperature is evident, along with an increase in the number of smaller clusters.

Four-, five-, and six-membered rings are the favored species at both 40 and 75 °C. A planar five-membered ring would have linear hydrogen bonds with optimal 108° for angles H···:O$'^{H}$ (thus centering the lone pair electrons between the donor H and acceptor O). Six-membered (planar) rings also have an excellent 120° linear hydrogen-bonding geometry. Four-membered rings formally make 90° angles, but as it is normal for the hydrogen to lay slightly off the O–O vector, tetramer ring angles of greater than 90° are permissible. If the hydrogens of a planar tetramer ring were 21° out of plane, the H···:O$'^{H}$ angle would be 111°. In the apparent trade-off between enthalpic and entropic factors, five-membered ring clusters are the more prevalent species at 40 °C (Figure 3, inset), whereas the four-membered rings are slightly more favored at 75 °C (Figure 4, inset).

It should be noted that "rings" are defined as polymeric species having at least one head-to-tail loop closure but they may also contain extended chain regions. Chains have no loop closures but may have branching. Thus a six-membered ring

(63) Saenger, W. *Ann. Rev. Biophys. Biophys. Chem.* **1987**, *16*, 93–114.

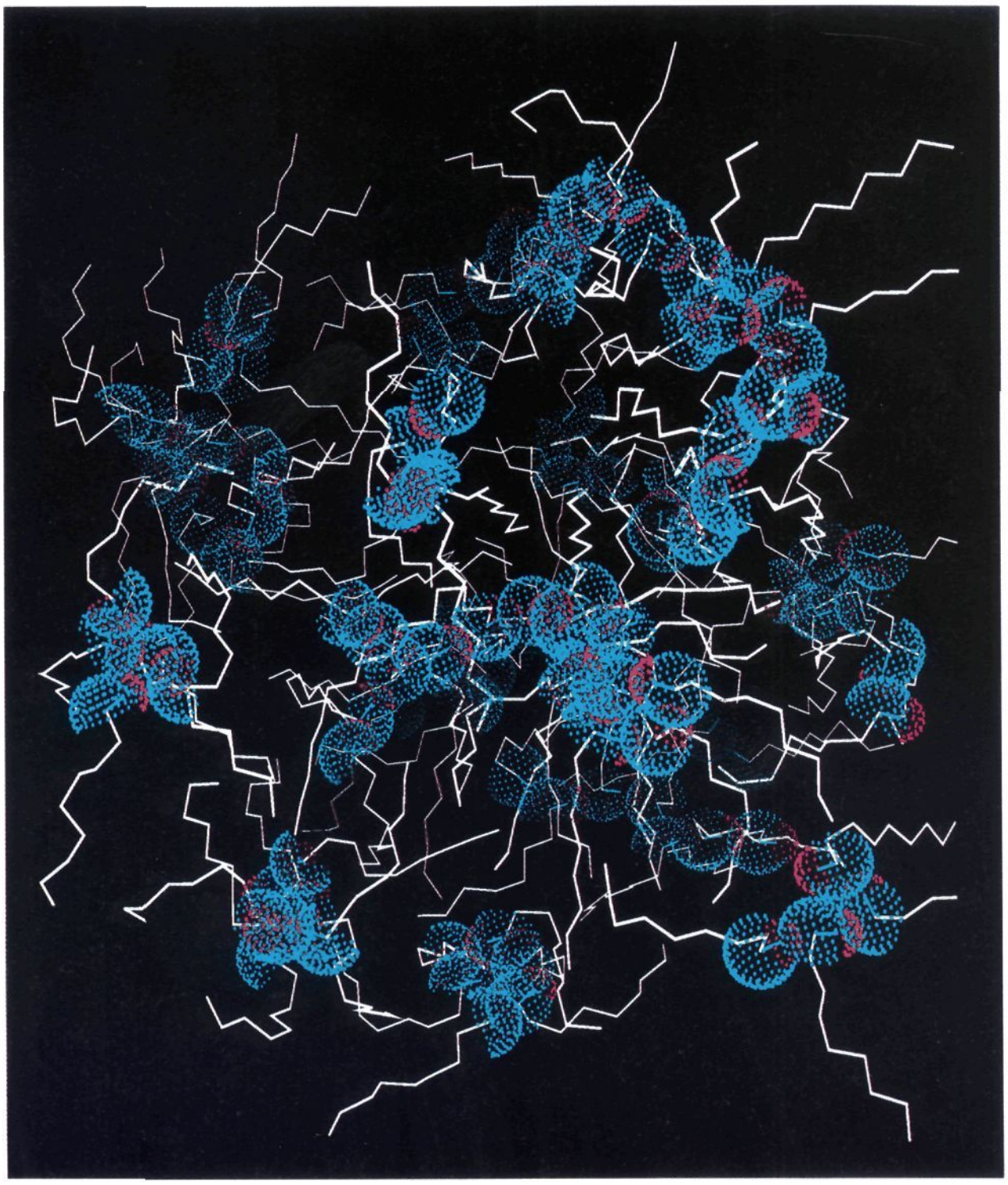

Figure 5. Pure 1-octanol clusters. Blue van der Waals radii represent oxygens, red represents hydrogens, and hydrocarbon tails are as white chains.

may be a closed loop of six hydrogen-bonded octanols, a closed loop of five octanols and one attached "tail piece" octanol hydrogen bonded to one of the ring members, or possibly a closed loop of four octanols and a single dimeric tail piece, or two monomeric tail piece octanols bound to different positions on the four-membered ring. As the number of molecules in a "ring" increases, the probability that the species is a simple closed loop decreases. However, *most* of the smaller ring structures, up to and including six- or seven-membered rings, are simple closed loops. Figure 5 illustrates aggregate formations in pure liquid 1-octanol media. The oxygen VDW surfaces are in blue, hydroxyl hydrogen surfaces are in red, and the alkyl tails are represented as white lines. The alkyl tails closer to the viewing eye are drawn "thicker". Although some short-to-medium-length polymeric chains are present, the majority of clusters seen in this particular example are small ring clusters forming a central hydroxyl core from which their alkyl chains radiate generally outward.

An equilibrium between short open chains and large ring or chain structures underlies the shift in the cluster-size distribution with temperature. In Figures 3 and 4 (main display), the upper solid line drawn through the main histogram indicates the contribution from species containing rings and the lower solid line indicates the contribution from open-chain species. Both rings and chains contribute significantly to the peak centered around five-membered species. At 40 °C, the excess of four-, five-, and six-membered structures is due mainly to the formation of rings. Aggregates (both rings and chains) of a size greater than say 20 molecules become less frequent with an increase in temperature. The equilibrium shifts toward the smaller species, including monomers, dimers, and trimers. At 40 °C (Figure 3, solid lines), there is always a higher occurrence of rings for cluster sizes greater than three members, whereas at 75 °C (Figure 4, solid lines), the occurrence of rings is higher than that of chains only for four-, five-, and six-membered structures. At the increased temperature, the number of chains in the peak area doubles but the ring contribution essentially remains balanced; both large chains and (especially) large rings are converted to small chains with an increase in temperature.

The MD results support experimental studies presenting evidence for a distribution of cluster sizes[60−62] rather than those which argue for a limited set of very few species.[58,59] Several studies have recently presented data in support of a hypothesis that 1-octanol consists almost exclusively of a monomer/tetramer (ring) equilibrium system, with perhaps a very low concentration of some other small species such as dimers.[58,59] Some of that data might now be reinterpretable in light of the new information from MD simulations presented here. Specifically, MD simulations find that monomers and tetramer (ring) structures are present but do not support the idea that these are the exclusive species present. Data presented by previous studies might also be interpreted as supporting the presence of two less specific

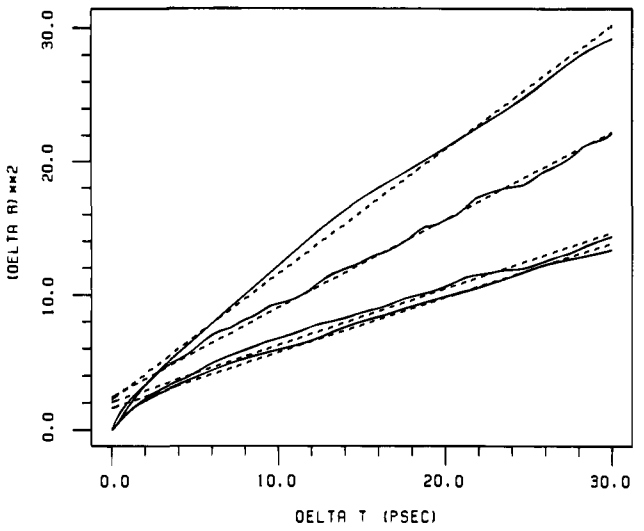

Figure 6. Plot of $\langle(\Delta r)^2\rangle$ versus Δt, where Δr is the difference in the position of the center of mass of a molecule at some time t and $t = 0$. Solid lines are actual data; broken lines are straight-line fits. The uppermost line is for pure 1-octanol at 75 °C. The lowermost line is for pure 1-octanol at 40 °C. Inner lines are for 40 °C hydrated 1-octanol, where the higher line represents the diffusion of saturation waters and the lower line represents 1-octanols in the presence of saturating waters. Data were gathered from multiple lag times of up to 30 ps over a 600 ps source trajectory and averaged over 250 molecules. Also see text.

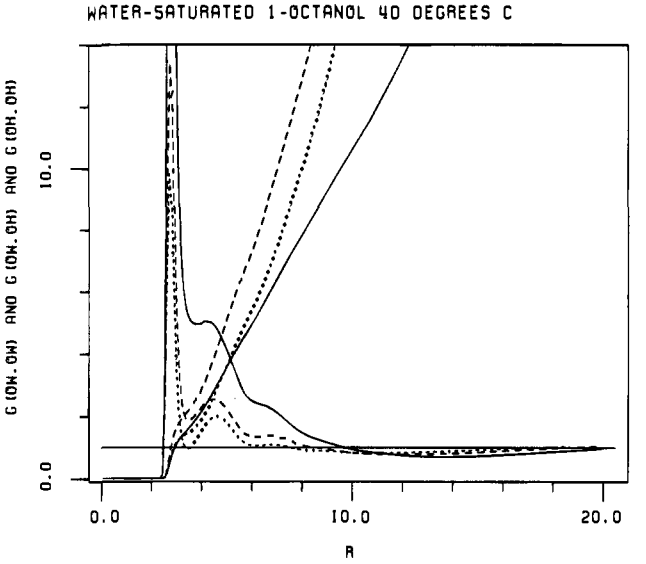

Figure 7. Radial pair distribution functions for water-saturated 1-octanol at 40 °C. Plots are $g(O_w,O_w)$ between water oxygens (solid line), $g(O_w,O_h)$ between water oxygen and octanol oxygen (broken, long dashes), and $g(O_h,O_h)$ between octanol oxygens (broken, short dashes). RDF $g(O_w,O_w)$ rises to $g = 26.6$ at $R = 2.7$ Å. Coordination number plots (number of pairwise contacts as determined by integrating the RDF) follow the same line designations. Data were collected over 2.5 ns MD (50 000 coordinate sets) as in Table 6.

hydroxyl species, namely H-free hydroxyls and H-bound hydroxyls. This would bring them into agreement with these MD studies as well as with other experimentalists[60-62] who have found evidence for the presence of several species, including monomers, small multimers, closed rings, and large hydrogen-bonded polymeric aggregates. These latter-mentioned experimentalists also demonstrate temperature-dependent changes in species' concentrations which parallel the MD results.

C. Self-Diffusion Coefficients. The three-dimensional self-diffusion coefficients were computed at 40 and 75 °C for pure 1-octanol by monitoring the displacement of a molecule as a function of time using the Einstein relation[64]

$$6D\delta t = \lim_{\Delta t \to \infty} \langle |\mathbf{r}_i(t + \Delta t) - \mathbf{r}_i(t)|^2 \rangle \qquad (7)$$

where D is the center of mass self-diffusion coefficient, $\mathbf{r}_i(t)$ are the molecular positions at time t, and Δt is the time interval between the initial position and the position at time t. An average $\langle(\Delta \mathbf{r})^2\rangle$ was computed for each of the 250 octanol molecules in a simulation, over a series of progressively longer lag time intervals and all choices of time origins taken from a 600 ps segment of MD trajectory. The results of the 250 separate molecular diffusional trajectories were then averaged to improve statistical accuracy.

Figure 6 is a plot of the average $\langle(\Delta \mathbf{r})^2\rangle$ versus Δt, shown for 40 and 75 °C, where multiple lag times, Δt's, of up to 30 ps were taken over the 600 ps "source" trajectory. The best least-squares-fit straight lines to each diffusion plot are also shown (broken lines). All points are contributed equally in the fitting; errors associated with the values given below are the standard errors of the respective regression coefficients (the slopes). The slopes of the plots are equal to $6D$. The plots in Figure 6 have reached a linear regime as evidenced by their unbiased random wavering about the fitted lines. The experimentally determined self-diffusion coefficients for pure octanol are 0.325×10^{-5} cm^2 s^{-1} at 40 °C and 0.85×10^{-5} cm^2 s^{-1} at 75 °C.[59] The two pure 1-octanol MD simulations (lower-most and upper-most curves) give $(0.68 \pm 0.01) \times 10^{-5}$ and $(1.55 \pm 0.01) \times 10^{-5}$ cm^2 s^{-1}, respectively, from the slopes of the fitted lines in Figure 6. Thus, modeled 1-octanol is about a factor of 2 times more diffusionably mobile than real 1-octanol, most probably because of the absence of explicit hydrocarbon hydrogens, thereby reducing intermolecular friction and entanglement.

The lower of the two inner curves (Figure 6) is for the diffusion of 1-octanol molecules in the presence of saturating waters, taken at 40 °C. The waters apparently "loosen up" the media, causing the octanols to diffuse very slightly more rapidly ($(0.70 \pm 0.01) \times 10^{-5}$ cm^2 s^{-1}) than in the pure liquid. The upper inner curve represents the diffusion of the saturating waters at 40 °C, which are quite mobile ($(1.10 \pm 0.01) \times 10^{-5}$ cm^2 s^{-1}) relative to the more sluggish octanols. As a point of reference, the experimental self-diffusion coefficient of pure liquid water[65] at 25 °C is 2.30×10^{-5} cm^2 s^{-1} and the calculated diffusion coefficient for model SPC water[32] at 27 °C is 3.6×10^{-5} cm^2 s^{-1}. The octanol-saturating waters are dramatically slowed by the presence of the long chains and the restricting hydrophobic regions.

D. Preferential Self-Solvation in Water-Saturated Octanol. The third level of structure in 1-octanol and water-saturated 1-octanol was designated as *regions of special character*. More specifically, there are regions containing relatively higher or lower concentrations of polar groups. Hydrophilic groups prefer to directly associate with or reside in the nearby vicinity of other hydrophilic groups; consequently, hydrophobic groups also tend to congregate. Amphiphilic-chain solvents, such as octanol, facilitate optimal alignment and association of "like" groups by forming aggregates resembling inverted micelles. A *region* can be further characterized as to its average "size", its degree of definition, its relationship to adjacent regions, and the effect of added saturating waters.

First, the average number of hydrogen bonds formed per molecule can be determined from the coordination number plots presented in Figure 7 for water-saturated octanol at 40 °C. The number of hydrogen-bonded partners that a given hydroxyl

(64) Allen, M. P.; Tildesley, D. J. *Computer Simulation of Liquids*; Clarenden Press: Oxford, U.K., 1987; pp 60, 204.

(65) Mills, R. *J. Phys. Chem.* **1973**, *77*, 685.

Table 6. Number of Interspecies Hydrogen Bonds in Water-Saturated 1-Octanol[a]

1st-shell neighbors	center O_{oct}	center O_{wat}
O_{oct}	1.48	2.19
	(1.63)	(2.81)
O_{wat}	0.73	1.61
	(0.58)	(0.99)
totals	2.21	3.80

[a] Values arrived at by integrating the appropriate RDF from 0.0 to 3.5 Å. System of 228 octanol molecules and 76 waters (40 °C). Parentheses indicate the number of hydrogen bonds which would result if hydroxyl pairing were random among all available hydrogen-bonding sites. Data gathered over 2.5 ns (50 000 coordinate sets).

group forms to each other species in its first solvent shell (0.0–3.5 Å between heavy atoms) is tabulated in Table 6. Each octanol forms 2.21 and each water forms 3.80 hydrogen bonds on average. Hydrogen-bonding sites are not fully saturated, but nearly so, especially for water. In Table 6, the numbers in parentheses are the numbers of hydrogen bonds which would be formed if hydroxyl pairing were random among the available hydrogen-bonding sites. For example, since there are $98 \times 3 = 294$ sites available for hydrogen bonds to octanols, a total of $(98 \times 3) + (26 \times 4) = 398$ possible sites (including waters), the number of "unbiased" octanol-to-octanol hydrogen-bond pairs would be $2.21 \times 294/398 = 1.63$. But on average, only 1.48 octanol-to-octanol hydrogen bonds form per octanol molecule; there is a 0.15 bond bias favoring octanol-to-water hydroxyl pairing. The octanol hydroxyl is slightly more stable when bound to a water than when bound to another octanol. For water there is a 0.62 hydrogen-bond bias for binding to other waters.

The water-saturated 1-octanol model reproduces the expected preferential self-solvation behavior of "like" groups, described in terms of local mole fractions. Marcus examined the incidence of preferential solvation in water-saturated 1-octanol using thermodynamics and quasi-lattice theory.[41] He predicted that the saturating waters would have a local excess mole fraction of neighboring waters in their first solvent shell as compared to the bulk mole fraction. At a saturation level where the bulk mole fraction of water X_{wat} is 0.250, Marcus predicted the local mole fraction of waters surrounding a given water would be 0.446, assuming water has four binding sites. This MD study (also with $X_{wat} = 0.25$) finds the average number of bound sites to be 3.80, and a given water binds to 1.61 other waters. The resulting local mole fraction is $1.61/3.80 = 0.424$, in close agreement with Marcus's prediction. Marcus also predicted a deficiency in the local mole fraction of waters around octanol molecules, 0.185. Table 6 reports 0.73 neighboring first-shell waters around a central octanol oxygen (from MD simulation). If we assume a total of four "binding" sites for octanol, as Marcus does, the MD simulations predict $0.73/4.0 = 0.183$ for the deficiency in the local mole fraction of waters around octanols. Clearly, waters most prefer to associate with other waters; octanols preferentially associate with other octanol molecules. The work of O'Connell and co-workers suggests similar conclusions.[9]

E. Inverted Micellar Bodies in Pure 1-Octanol. The tendency to form small inverted micellar-like regions prevails throughout both pure 1-octanol and water-saturated 1-octanol. These aggregates might be termed mini-micelles. It is clear from Figure 1 than a given hydroxyl oxygen (located in the center of a sphere at $R = 0$) is immediately surrounded by a polar region of high definition, as indicated by the region of peaks extending out to about $R = 5.5$ Å. Figure 8 is a closeup of the curves first presented in Figure 1. It focuses on the dip below $g = 1.0$ in the hydroxyl atoms' RDFs g(O,O) (solid line) and g(O,H) (dashed) seen from about $R = 5.5$ Å out to about

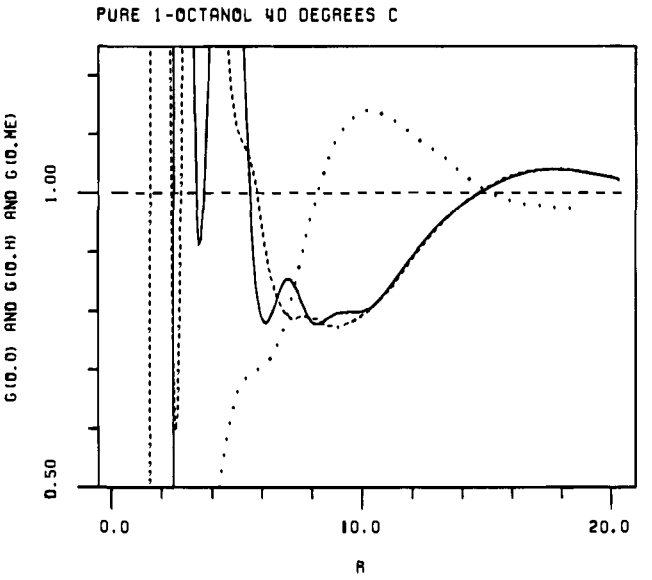

Figure 8. Closeup of radial pair distribution functions in pure 1-octanol. Plots are g(O,O) between hydroxyl oxygens (solid line) and g(O,H) between the oxygen and surrounding hydroxyl hydrogens (broken line). The dotted line is g(O,Me). Data were obtained from averaging 250 molecules of pure 1-octanol at 40 °C, over more than 30 000 coordinate sets, about 2 ns MD.

$R = 14.75$ Å. This dip indicates a nonpolar area bereft of hydroxyl groups. The hydrocarbon tails reside here, as confirmed by g(O,Me), the dotted curve, peaking at $R = 10.25$ Å. The g(O,O) curve (solid) then raises above $g = 1.0$ at $R = 14.75$ Å, cresting at $R = 17.75$ Å. This rise above $g = 1.0$ at so long a distance from the central hydroxyl oxygen is not a statistical anomaly; it is the detection of the polar region at the core of the adjacent mini-micelle(s). Notice that when hydroxyl groups *are* present in the nonpolar dip area, they reside at very specific locations (peaking at about $R = 7.0$ and $R = 9.0$ Å). These intermittent hydroxyl peaks in the hydrocarbon trough of the RDF may be interpreted as sequentially ordered hydroxyls in a hydrogen-bond-linked polymeric chain stretching through or alongside a nearby nonpolar region. This average structure also results from the fact that most hydroxyls are located at the micellar polar/nonpolar boundaries, with neighboring hydroxyls packed to one side, and the nonpolar milieu off to the other direction. If the polar cores of the mini-micelles are thought of as essentially spherical, then most "core" hydroxyls lay nearer to the outer radius of a core than to its exact center.

Figure 9 shows three pure 1-octanol RDFs, two involving hydrocarbon-to-hydrocarbon pairs, g(Me,Me) and g(Me,ML), and also g(Me,O) which is equivalent to g(O,Me). The corresponding coordination number plots are also shown. We can declare the first "hydrophobic" solvation shell to have a center-to-center radius of 4.38 Å since united atom methyls or methylenes have optimal van der Waals contact radii of 2.19 Å (see Table 2) and are uncharged. On average, there are 1.0 methyl, 0.3 oxygens, and 3.0 methylenes within the 4.38 Å contact distance of a given methyl group.

We can see the partitioning of the media into polar and nonpolar regions from the perspective of an octanol methyl group (at $R = 0$) in Figure 9. The oscillating contours of g(Me,-Me) (solid line) demonstrate well-defined structuring of the nonpolar milieu about the methyl group. There is one neighboring methyl group in the near-shell ($R = 4.25$), followed by shells which are alternatively rich in methyls (peaks at $R = 9.0$, and beyond $R = 16.0$ Å) or depleted of methyl groups (troughs at $R = 7.25$ and 11.5 Å). Turning to the g(Me,O) curve (long dashes), the coordination number reaches 1.0 oxygen at $R = 5.35$ Å. The region from $R = 8.25$ to $R = 16$ Å, where

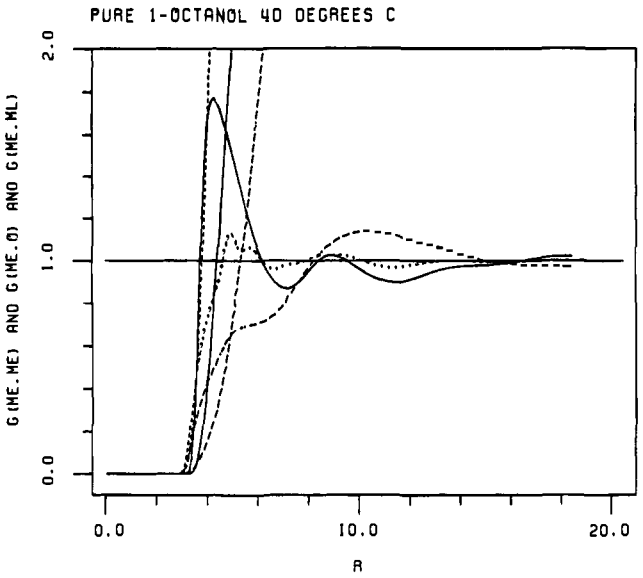

Figure 9. Radial pair distribution functions in pure 1-octanol. Plots are g(Me,Me) between end methyls (solid line), g(Me,O) between end methyls and hydroxyl oxygens (broken line, long dashes), and g(Me,-ML) between end methyls and methylenes (short dashes). Data were collected as in Figure 8.

the g(Me,O) curve raised above 1.0, is rich in polar oxygen groups, as evidenced by the peak in g(Me,O), while depleted of both methyl and methylene groups. At about $R = 16$ Å, the local concentration of methyl groups again increases (as the concentration of oxygens decreases). There must be a very significantly enhanced presence (methyls) or deficit (oxygens) of these groups at this radial distance for the appearance of a signal at other than $g = 1.0$.

The approximate size of a mini-micelle and the average number of molecules composing it can be estimated from the distances between regions indicated by the RDFs. First, we approximate the diameter of the polar core. Beginning with g(O,O) (Figure 8, solid), an octanol oxygen positioned at $R = 0$ sees (on average) a polar-enriched region of length 5.5 Å. This should not be interpreted as a spherical region of radius 5.5 Å, as most hydroxyls lay near the periphery of a hydrophilic core. The RDF-indicated polar zone is more representative of oxygens "looking across" the polar core than it does from centralized oxygens which look out over an encircling polar sphere. We can conclude that a pure 1-octanol polar micellar core region has a (atom center to atom center) diameter of at least 5.5 Å, and somewhat more, but less than 11.0 Å (if 5.5 Å were taken as a radius). If the second enriched polar region (representing adjacent polar cores) in the g(O,O) plot is symmetric about $R = 17.75$, it would span about 6.0 Å. But the system was not of sufficient size to confirm $R = 17.75$ as the true crest; an RDF trails off as R approaches one-half the length of the simulation box (which is 20.35 Å here). Alternatively, in the g(Me,O) plot (Figure 9, long dashes), a complete enriched-polar-region signal is available from $R = 8.25$ to $R = 16.0$ Å, at the boundary where polar and nonpolar regions abut. Note the polar region's span of $16.0 - 8.25 = 7.75$ Å is not symmetric about its peak at $R = 10.25$ Å. This also leads to the interpretation that the correct overall span of the "far" polar-enhanced region of the g(O,O) plot in Figure 8 (at $R > 14.75$) may be greater than 6 Å; more precisely, the g(O,O) peak should be shifted to somewhere within the range 17.75−18.6 Å.

Let us piece together these several clues regarding the diameter of the polar core. The "near" polar-enriched region of g(O,O) indicates that the diameter is greater than 5.5 Å, but less than 11.0 Å, the incomplete "far" polar peak indicates at least 6.0 Å, and the polar-enriched region of g(Me,O) indicates a core diameter of 7.75 Å. All of these indicators are mutually consistent, leading to 7.75 Å as an estimate of the average diameter of the polar core region formed when 1-octanol aggregates into inverted mini-micelles.

The overall micellar diameter can be approximated as the distance between polar cores, 17.75−18.6 Å on average in pure 1-octanol (from Figure 8, solid, and its far polar region peak correction determined from Figure 9). This gives an average micellar volume of 2928−3369 Å^3. Dividing this by the volume per molecule in the simulation (see Table 3), 265.2 Å^3, yields 11.0−12.7 molecules per mini-micelle.

The hydrocarbon chain portion of an octanol molecule can extend about 9.5 Å, and a significant number of the chains are fully extended (Table 4). Because there is about one extended chain's length between the hydrophilic regions, the chains from adjacent mini-micelles may either avoid each other or interdigitate to some extent. Figure 9 indicates that a terminal methyl group makes a van der Waals contact with 0.30 oxygens (coordination number integration line taken at $R = 4.3$ Å, long dashes). This could be interpreted to mean that about one of every three methyl groups reaches far enough to contact one of the hydroxyl oxygens on the periphery of an adjacent mini-micelle's polar core. Some of the hydrocarbon tails from octanol molecules in neighboring aggregates must be close packed to facilitate this. This is visually evident in color Figure 5, where the clustered octanol hydroxyl oxygens are represented as blue van der Waals surfaces and the nearby hydrocarbon tails as white chains. At this point we have a clear and detailed description of the internal structure of pure liquid 1-octanol.

F. The Effect of Saturating Waters on Liquid Structure. Do saturating waters disrupt or significantly alter 1-octanol's internal structure? In the binary octanol/water media, the strongly attractive water molecules cause other hydroxyl groups to gather around them, with a special bias for other water hydroxyls. Therefore, when water partitions into octanol, it should be expected to lodge in and perhaps promote or stabilize polar cores, causing larger and more distinctive hydrophilic regions than seen in pure 1-octanol.

There are several notable features in the cluster-size histogram for water-saturated 1-octanol presented in Figure 10. Note the flatness of the curve compared to pure 1-octanol (Figure 3) and the presence of many clusters larger than even 80 molecules. Water molecules pack into "tight" spaces in the media (where a bulky octanol molecule could not fit), promoting a much more extensive hydrogen-bonding network and facilitating interconnections or "bridging" of large aggregates. Recall (Figure 3) that in pure 1-octanol the plot of chain species trails off with 70-mers at 40 °C and (Figure 4) with 40-mers at 75 °C. The long-chain curve trails off with 20-mers in hydrated 1-octanol at 40 °C (Figure 10, main histogram, inscribed solid line peaking at $N = 1.0$). Long extended polymeric hydrogen-bonded open chains are rare in the presence of saturating waters. Notice also (Figure 10) that, even with the noiser statistics, four- and five-membered species are apparently still slightly favored while dimers and trimers are not.

The RDFs presented for water-saturated 1-octanol in Figure 7 are very similar in general contour to those seen for pure 1-octanol (Figure 1). In Figure 7, there is a more highly structured polar region in the three hydroxyl oxygen RDFs, $g(O_w,O_w)$, $g(O_w,O_h)$, and $g(O_h,O_h)$. The first peak of $g(O_w,O_w)$ (solid line) rises to $g = 26.6$ at $R = 2.7$ Å (lopped off in Figure 7). Even with the relatively few waters in the system (76 versus 228 octanols), the probability of finding the waters close to other waters, in the polar core region, is very high. Where the pure 1-octanol RDF (Figure 1) indicates *two* polar-enriched solvent shells ($g > 1.0$) near a given alkoxyl group, the water-saturated

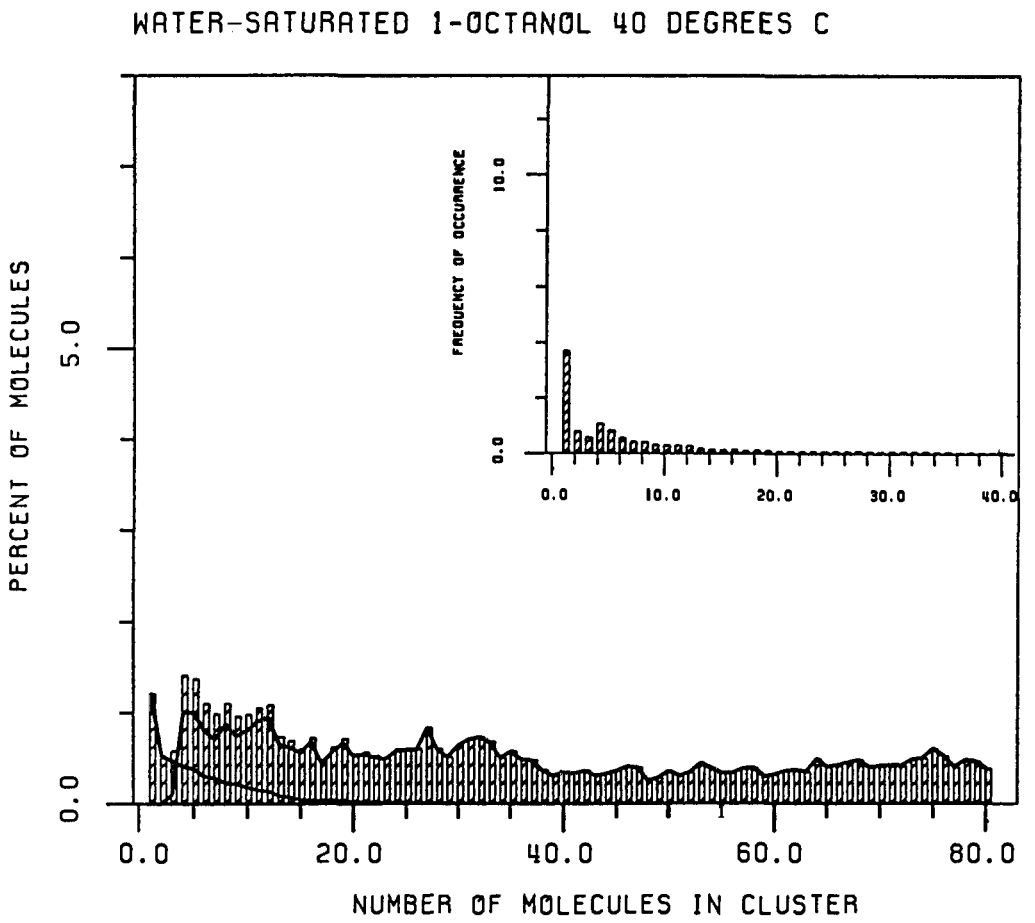

Figure 10. Frequency distribution of clusters of various sizes in hydrated 1-octanol at 40 °C. The main display reports the percent of molecules which participate in a cluster of a given size. The inset reports the actual number of clusters of a given size found in a periodic box of 228 1-octanol molecules and 76 waters. The solid line following the histogram's crest indicates the contribution from species containing rings; the solid line peaking at 1.0 indicates the contribution from open-chain species. Data collection was as in Figure 7.

1-octanol curves (Figure 7) indicate *three* polar-enriched solvent shells adjacent to a given water or alkoxyl group. The hydrated-octanol RDF curves do not dip below $g = 1.0$ until about $R = 9.0$ Å (Figure 7), whereas in pure 1-octanol the dip begins at $R = 5.5$ Å (Figure 1).

Figure 11 (a closeup of Figure 7) shows $g(O_w,Me)$ (dots) crossing over the $g(O_w,O_h)$ curve (broken, long dashes) at about $R = 9.0$ Å, while the $g(O_h,O_h)$ (broken, short dashes) and $g(O_w,O_w)$ (solid) curves cross the $g = 1.0$ boundary to either side of this. The $g(O_w,Me)$ line (dots) rises above $g = 1.0$ at $R = 9.5$ Å, indicating the prominence of nonpolar groups, confirmed by the drop of $g(O_w,O_w)$ (solid) below $g = 1.0$. In water-saturated 1-octanol, then, the polar core region is filled with waters and is overall larger than in pure 1-octanol. By following the rationale used above in analyzing pure 1-octanol, we can conclude that the core region has a diameter greater than 9.5 Å but less than 19.0 Å (if 9.5 Å were taken as a radius). Notice that R (in Figure 11) just barely extends far enough ($R = 20.0$ Å) to show the appearance of the neighboring polar core(s), beginning at about 18.5 Å.

The diameter of the hydrated 1-octanol's polar core can be more closely estimated from the RDFs in Figure 12. A methyl group located at $R = 0.0$ sees an enriched polar area (dashed lines) beginning at $R = 9.0$ and ending at about $R = 19.0$ Å, where a "far" methyl enrichment begins. This means the polar core has a 10.0 Å diameter, consistent with the range indicated by Figure 11. It is also clear from the Figure 11 RDFs that, while water molecules are more concentrated in the central part of the polar core (peak near $R = 12$, short dashes), they are present throughout the entire core region, although along the

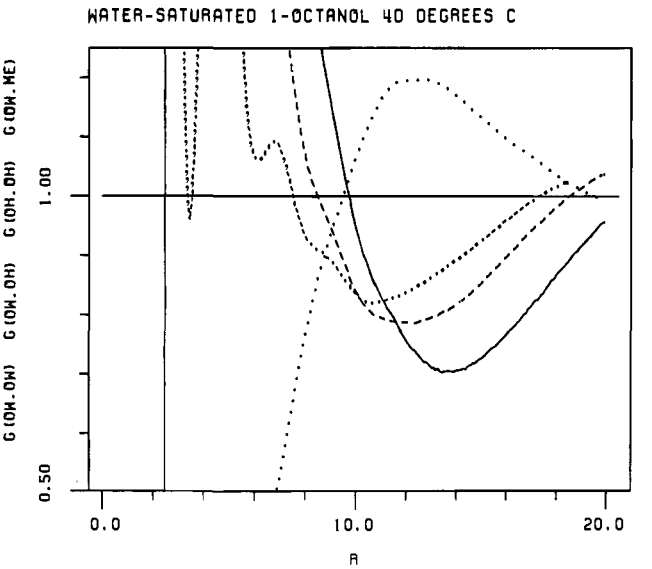

Figure 11. Closeup of radial pair distribution functions for water-saturated 1-octanol at 40 °C. Plots are $g(O_w,O_w)$ between water oxygens (solid line), $g(O_w,O_h)$ between water oxygen and octanol oxygen (broken, long dashes), and $g(O_h,O_h)$ between octanol oxygens (broken, short dashes). The dotted plot is $g(O_w,Me)$. Data were collected as in Figure 7.

core's perimeter the primary residents are octanol hydroxyls (shoulder near $R = 6$, long dashes).

We can estimate the overall micellar diameter as the distance between the polar cores by using information from both the $g(O_w,O_h)$ curve in Figure 11 and the $g(Me,O_h)$ curve in Figure 12. Figure 12 shows $g(Me,O_h)$ and $g(Me,O_w)$ (long and short

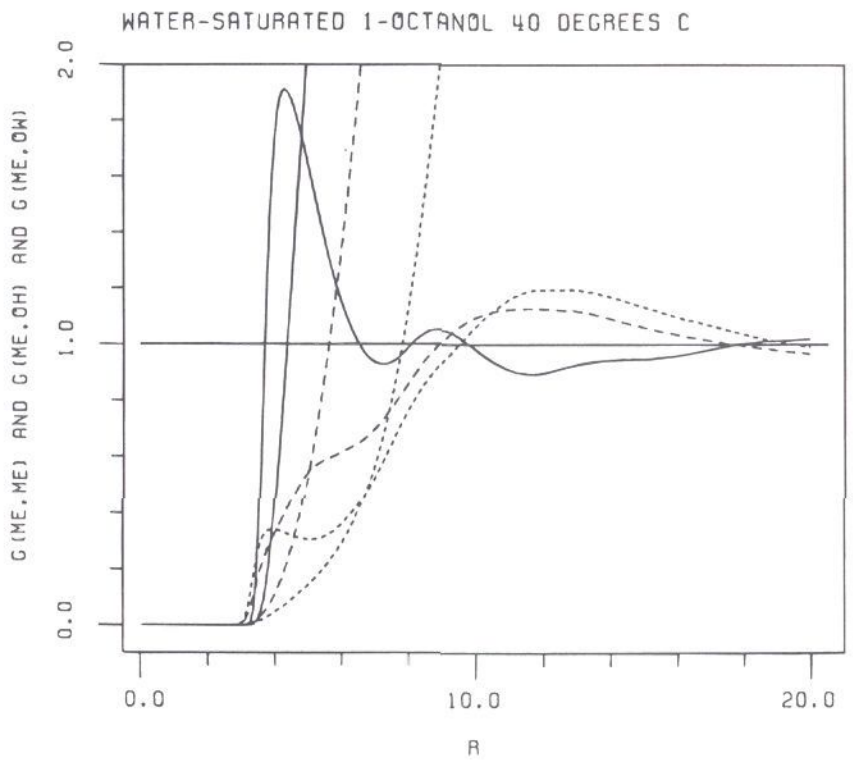

Figure 12. Radial pair distribution functions in hydrated 1-octanol. Plots are g(Me,Me) between end methyls (solid line), g(Me,O_h) between end methyls and hydroxyl oxygens (broken line, long dashes), and g(Me,O_w) between end methyls and water oxygens (short dashes). Data were collected as in Figure 7.

broken lines) peaking about 3.0 Å beyond their $g = 1$ crossing points at $R = 9.0$ and 9.5 Å. Appending this 3.0 Å to the $g = 1$ crossing point on $g(O_w,O_h)$ at $R = 18.5$ Å in Figure 11 enables the determination of the polar core-to-core distance. The overall micellar diameter is thus estimated to be about 21.5 Å in water-saturated 1-octanol. This is 3.0 Å longer than in pure 1-octanol. Since the polar core diameter is only 2.25 Å longer than in pure 1-octanol, the hydrocarbon chains apparently interdigitate to a slightly lesser extent (less by $3.0 - 2.25 = 0.75$ Å) when water is present.

Figure 13 illustrates how water-saturated 1-octanol separates into preferentially polar or nonpolar regions, forming inverted micellar aggregates. These water-containing aggregates have a more well-defined micellar structure than that seen in the pure 1-octanol clusters (Figure 5). There is a notable absence of long hydrogen-bonded chains in Figure 13. Waters pack in among the octanol hydroxyls. The long polymeric hydrogen-bonded chains common in pure 1-octanol are apparently less favored under hydrated conditions. Octanol hydroxyls are drawn in to clusters at unbound water sites. An interesting alternative hydrophilic core motif can be seen in Figure 14, which illustrates "hydrophile channels", elongated micellar bodies forming cylindrical regions of hydrophiles, water hydroxyls and alkoxyl groups, with radially extending hydrocarbon tails. The hydrophile channels appear to be made up of two or more smaller micellar bodies with joined hydroxyl regions.

IV. The Partitioning of Small Solutes in Hydrated Octanol

1-Octanol is the most frequently used solvent in partitioning studies. Why is octanol such an exceptionally good analog for the biophases?

The above analysis of the internal structural features of water-saturated octanol media has helped to clarify the mechanism underlying this capability. Water-saturated 1-octanol has preferentially aqueous or aqueous-like regions, the polar cores

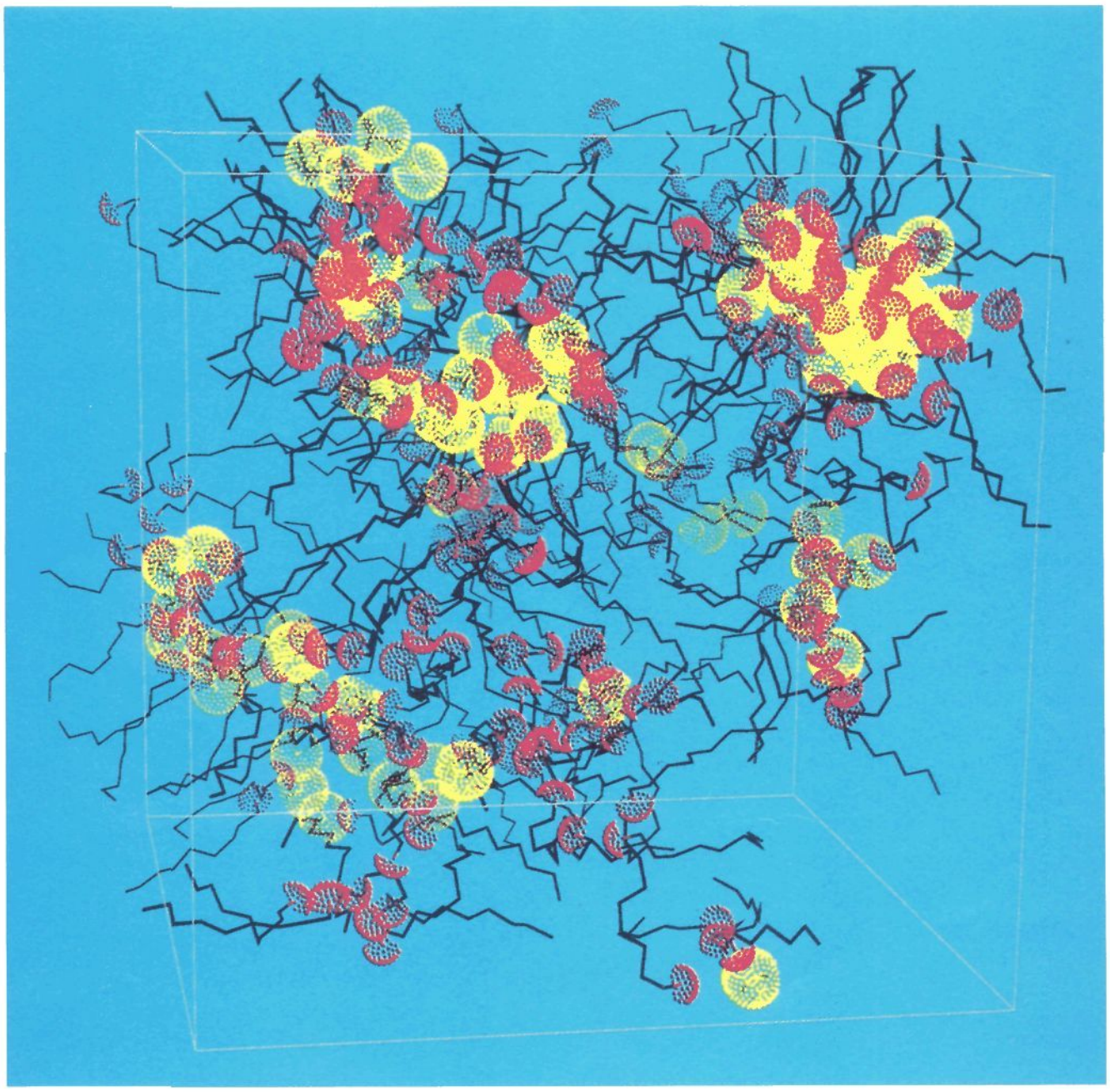

Figure 13. Water-saturated 1-octanol micellar aggregates. Yellow VDW radii represent water oxygens, red represents octanol hydroxyl hydrogens, and hydrocarbon tails are shown as black chains.

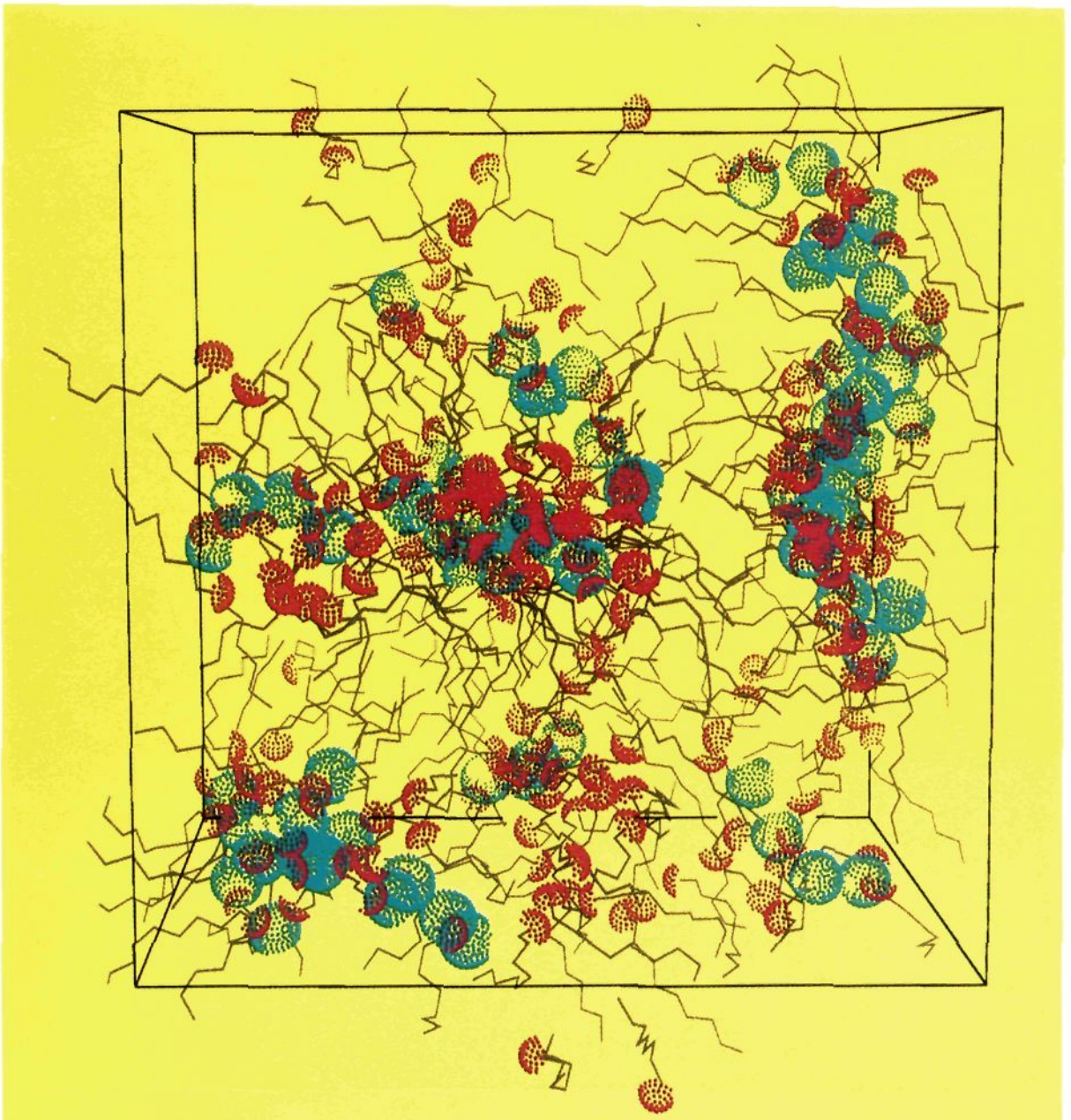

Figure 14. Hydrophile columns in water-saturated 1-octanol. Blue VDW radii represent water oxygens, red represents octanol hydroxyl hydrogens, and hydrocarbon tails are shown as black chains.

of inverted-micellar bodies. 1-Octanol's alkyl tails congregate outside these polar regions. A drug molecule can partition between these opposing polar/nonpolar regions, selectively migrate to a preferred locale, and exhibit a characteristic residence time, somewhat analogous to the way drugs partition with respect to the aqueous/lipidic compartmentalization of body tissues. One would expect hydrophilic solutes or hydrophilic moieties to preferentially take up residence in or near the polar core of an inverted mini-micellar region. Similarly, a hydrophobic solute or a hydrophobic moiety might be expected to migrate preferentially to the hydrocarbon-rich alkyl tail regions. An amphiphilic solute (most drugs and metabolites) would be expected to prefer some compromise, perhaps by positioning across the core/periphery regional boundaries of inverted-micellar aggregates.

The difference in the logarithm of the octanol/water partition coefficients $\Delta\log(K_{O/W})$ was computed for the aromatic solutes phenol and benzene.[36] The octanol solvation contribution to an octanol/water partition coefficient was calculated from data generated by high-resolution MD free-energy perturbation (FEP) simulations of a solute bathed in hydrated octanol media. Previously, investigators have reported $\Delta\log(K_{O/W})$ studies for small solutes in carbon tetrachloride[66] and chloroform.[67] The method we used to compute the relative octanol/water partition coefficient is only briefly described here. Further analyses here consider the solute/solvent interactions, the orientational relationship of the solutes to the solvent, and the differential positioning of the solute in regions of preferentially polar or nonpolar character.

The thermodynamic and structural aspects of small-molecule partitioning between water and water-saturated octanol were examined by carrying out an MD/FEP study of benzene and phenol at 37 °C. The following thermodynamic cycle was used:

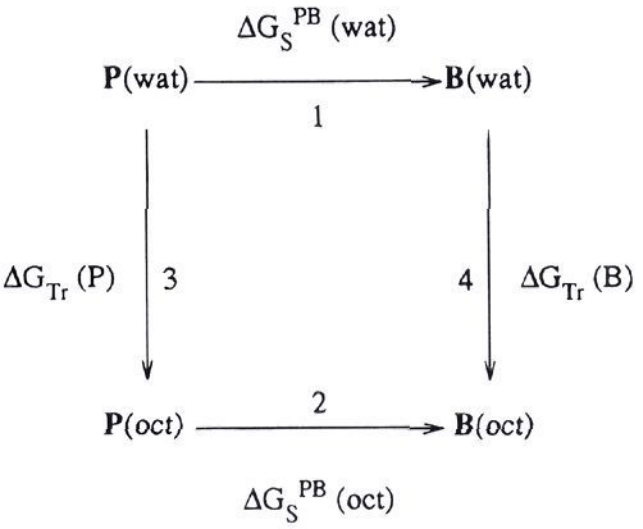

The difference in the aqueous solvation free energies of benzene (**B**) versus phenol (**P**) was computed using FEP via path 1.

In brief, the Hamiltonian of the system is smoothly perturbed so that the molecular parameters describing benzene are gradually mutated into parameters describing phenol, i.e. the hydroxyl group of the phenol is converted into a benzene ring hydrogen (and vice versa for the reverse perturbation) over 2.6 ns trajectories. The difference in the free energy of solvation

(66) Essex, J. W.; Reynolds, C. A.; Richards, W. G. *J. Chem. Soc., Chem. Commun.* **1989**, 1152−1154.

(67) Jorgensen, W. L.; Briggs, J. M.; Contreras, M. L. *J. Phys. Chem.* **1990**, *94*, 1683. Dunn, W. J., III; Nagy, P. I. *J. Comput. Chem.* **1992**, *13*, 468.

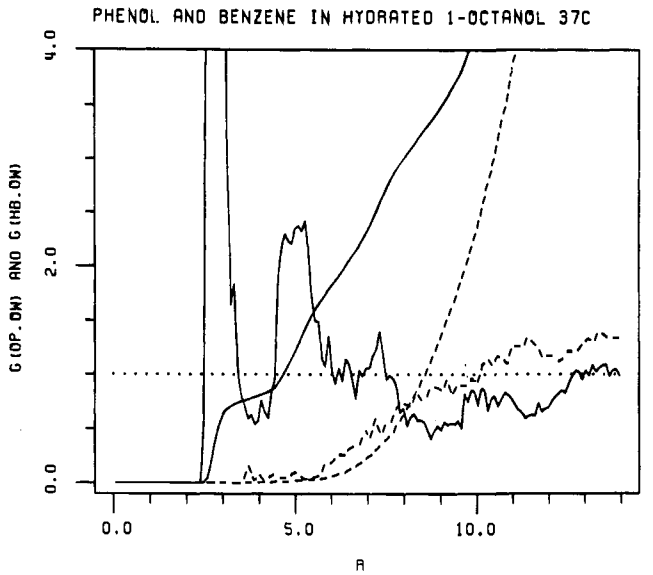

Figure 15. RDFs: phenol/benzene against water oxygen; $g(O_p,O_w)$ (solid line) and $g(H_b,O_w)$ (broken line), and coordination number plots. Data were collected over 2000 coordinate sets.

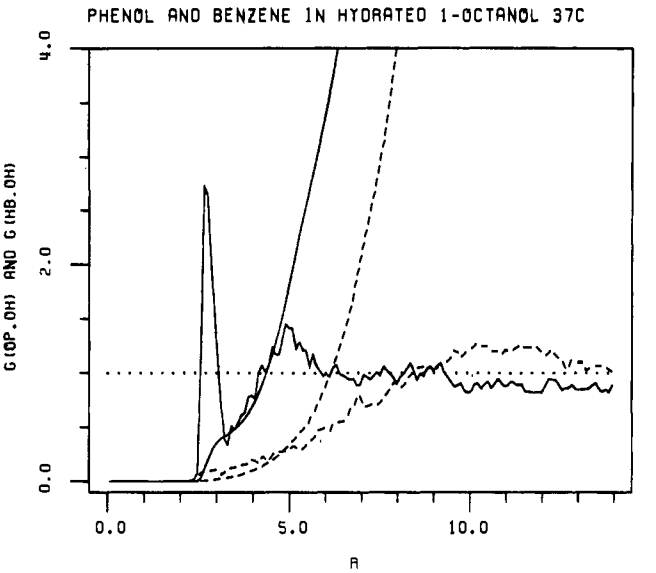

Figure 16. RDFs: phenol/benzene against octanol oxygen; $g(O_p,O_h)$ (solid line) and $g(H_b,O_h)$ (broken line), and coordination number plots. Data were collected as in Figure 15.

in water-saturated octanol (benzene versus phenol) was computed via path 2. The free energy of transfer of benzene or phenol from water to hydrated octanol (paths 3 and 4) would be too complex to compute directly, requiring the juxtaposition of the two bulk medias, an interface, and extended sampling over multiple solute transfer vectors. Instead, the following relationship was used:

$$\Delta G_S^{BP}(\text{oct}) - \Delta G_S^{BP}(\text{wat}) = \Delta G_{Tr}(\mathbf{B}) - \Delta G_{Tr}(\mathbf{P}) = \Delta\Delta G_{Tr}^{BP} \quad (8)$$

The FEP computational result in pure SPC water (path 1) was ΔG_{aq}(benzene→phenol) = −4.89 ± 0.20 kcal/mol. This compares well with the value obtained by Jorgensen[35] for the similar TIP3P water model, −5.2 ± 0.2. Subtracting the FEP-computed value in water-saturated octanol, $\Delta G_{oct/wat}$-(benzene→phenol) = −3.80 ± 0.35, gives −1.09 ± 0.55 kcal/mol for the difference in solvation free energies of benzene and phenol in hydrated octanol versus pure water. This is equivalent to the difference in their transfer free energies by eq 8. By converting this number through the formula relating free energies of solvation to octanol/water partition coefficients

$$\Delta\Delta G_{\text{transfer}}^{BP}(\text{oct/wat}) = -2.303RT\,\Delta\log(K_{o/w}) \quad (9)$$

gives the computed value of $\Delta\log(K_{o/w})$ as −0.76 ± 0.39 for benzene versus phenol. This compares to the experimentally measured $\Delta\log(K_{o/w})$ for benzene versus phenol, −0.67, at 25 °C, obtained from the difference of the experimental[68] absolute $\log(K_{o/w}(\text{benzene}))$, 2.13, and $\log(K_{o/w}(\text{phenol}))$, 1.46. The experimental relative partition coefficient is placed well within the standard deviation range resulting from the FEP calculations, giving very close agreement between the experimental and calculated values. The slight temperature difference at which coefficients were determined computationally versus experimentally has negligible influence over the relative partition coefficient.

Issues of protocol, sampling, and convergence in these FEP studies are discussed in detail in the forementioned publication, which also treats the issue of parallel processing in FEP calculations.[36] Extensive sampling was performed, giving the phenol and benzene solutes an opportunity to optimally locate

(68) Fujita, T.; Iwasa, J.; Hansch, C. *J. Am. Chem. Soc.* **1964**, *86*, 5175.

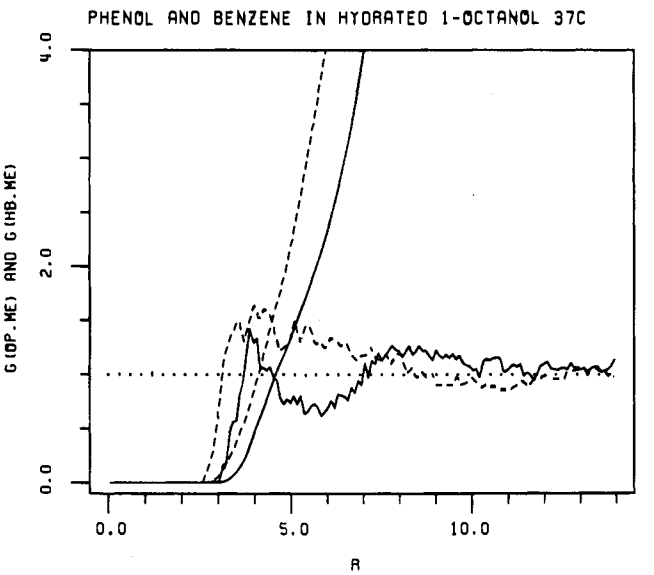

Figure 17. RDFs: phenol/benzene against octanol methyls; $g(O_p,M_e)$ (solid line) and $g(H_b,M_e)$ (broken line), and coordination number plots. Data were collected as in Figure 15.

and orient within the heterogeneous binary media. Two-thousand coordinate sets were saved from each of the $\lambda = 0$ and $\lambda = 1$ FEP end-state trajectories (i.e., "pure" benzene and "pure" phenol in hydrated 1-octanol). From these trajectories, solute−solvent RDFs were generated. Solute−solvent RDFs are less statistically accurate than solvent−solvent RDFs as only a single solute molecule is present to provide data.

The following structural analysis indicates that phenol resides near the interface zone on average, providing a clear molecular-level rationale for why phenol is a "surface active" molecule. Three solute−solvent RDFs are reported in Figures 15, 16, and 17. In all of these plots, the solid line refers to an RDF where the phenol hydroxyl oxygen, O_p, is central (at $R = 0$), and the dashed line refers to cases where the benzene ring hydrogen, H_b, (which substitutes for the phenol oxygen) is central. The corresponding coordination plots have the same line types. In Figure 15, the interaction of the solute groups with octanol's hydrating-water oxygens is represented. Clearly, the phenol hydroxyl is positioned near a polar zone in the media. From the (solid) integration curve we see that 0.75 near-shell hydrogen bonds are made with a hydrating water. The first peak in

$g(O_p,O_w)$ (solid) reaches 18.6 at $R = 2.75$. It was also determined, by integrating $g(H_p,O_w)$, an RDF (not shown) involving the phenol hydroxyl hydrogen, that 0.36 of this O_p-O_w bond has the phenol hydroxyl donating to the water oxygen. So, to achieve its 0.75 hydrogen bond, the phenol oxygen donates about half of it to a water and accepts the other half from a water. There are also a second water (peak at $R = 5.0$) and third water (peak at $R = 7.5$) near the phenol hydroxyl O_p. Beyond 7.5 Å, a polar-depleted region is indicated.

Figure 16 (solid integration line) shows 0.48 hydrogen bond between the phenol O_p and octanol O_h hydroxyl oxygens, 0.30 of which is an O_p donator (determined from $g(H_p,O_h)$, not shown). The binding octanol hydroxyl is in the vicinity of other octanol hydroxyls and also the hydrating waters shown in $g(O_p,O_w)$ (Figure 16). Beyond $R = 9.5$, Figure 16 shows a polar-depleted region. Bearing in mind the internal structure of water-saturated 1-octanol, namely the inverted micellar aggregates with polar cores of 10.0 Å diameter. it can be concluded that, on average, phenol's hydroxyl group lodges at the periphery of such a polar core. Figure 17 (solid line) shows 0.38 methyl groups within VDW contact distance (3.91 Å) of O_p. This signal is likely from a nearby alkyl tail which packs in around the benzene ring.

The benzene molecule centralizes among octanol's hydrocarbon tails in a nonpolar region that is broader than the average found in the bulk media. The benzene lodges in a region having a diameter at least as wide as 12 Å *plus* the size of benzene itself. Turning our attention to the benzene ring hydrogen H_b in Figures 15–17, no polar-enriched zone is closer than 9 Å (broken RDF lines in Figures 15 and 16). There is a region enriched in methyl groups beginning at the H_b VDW contact distance and extending to about 9 Å (Figure 17, broken). This is very interesting in light of our having demonstrated that the entire hydrophobic region between adjacent mini-micelles in hydrated 1-octanol spans 11.5 Å on average (21.5 (total) − 10.0 (core)). If benzene were positioned along the periphery of a nonpolar zone, it would also be near the abutting polar region. But, on average, H_b does not encounter even a single hydroxyl oxygen inside a radius of 6 Å (see Figure 16, broken coordination plot), and since all six of benzene's Hb atoms are equivalent, none of them are any nearer to a polar region.

It is gratifying that MD simulations can reproduce a molecular level effect such as the mediation of the nearby octanol/water solvent configuration by a single hydrophobic solute as small as a benzene. The hydrated-octanol media accommodates this hydrophobic solute by configuring a hydrocarbon-enriched solvation shell around it. This undoubtedly bears on the accurate computation of $\Delta\log(K_{O/W})$. Hydrated octanol may form various solvent shell configurations, depending on the nature of the molecule being solvated.

V. Dielectric Phenomena in Modeled Pure 1-Octanol

The value ϵ_0 was calculated for modeled pure 1-octanol at both 40 and 75 °C. The reaction field method described above is applicable only for homogeneous isotropic systems (of uniform composition) and therefore would not be appropriate for computing dielectric quantities in a small finite sample of binary media like water-saturated octanol. Figure 18 is a plot of the convergence of ϵ_0 versus time. Apparently, convergence is being approached near $\epsilon_0 = 5.1$ at 40 °C and $\epsilon_0 = 4.2$ at 75 °C, although longer simulations would be required for confirmation. Even though these simulations covered several nanoseconds, insufficient sampling could result in incomplete convergence in properties such as ϵ_0 and τ_1 relaxation, although it appears that the values for ϵ_0 are in the range from 4 to 6 for this model. The computed static dielectric constants, 5.1 and

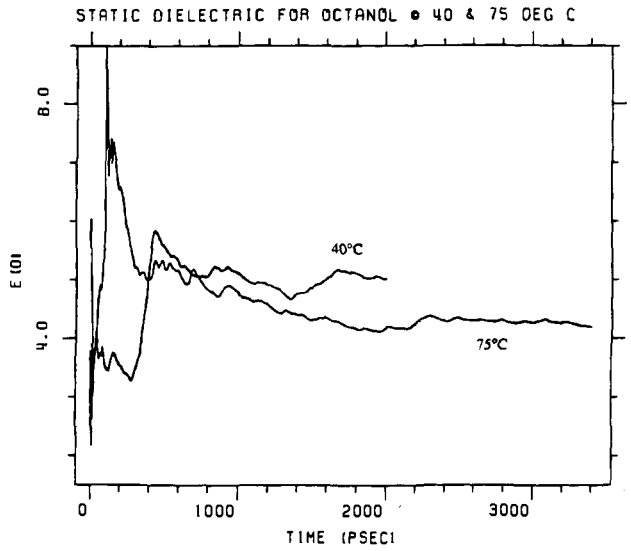

Figure 18. Plots of the cumulative static dielectric constant, ϵ_0, versus time in picoseconds. The upper line results from 2.0 ns MD of pure 1-octanol at 40 °C. The lower line results from 3.3 ns MD of pure 1-octanol at 75 °C.

4.2, are in qualitative agreement with the experimentally observed values, 8.7 (40 °C) and 6.1 (75 °C). As a point of reference, MD calculations of water's static dielectric constant have given $\epsilon_0(298\ K) = 35$ for MCY water,[43] $\epsilon_0(293\ K) = 53$ for TIP4P water,[69] $\epsilon_0(298\ K) = 72$ for SPC water,[70] $\epsilon_0(298\ K) = 70.7$ for SPC/E water,[71] $\epsilon_0(300\ K) = 82.5$ for flexible SPC water,[42] and $\epsilon_0(293\ K)$ ranging from 21 to 97 for TIP4P water depending on the smoothing function used at the spherical interaction cutoff boundary.[72] These various results compare with the experimental[73] value of $\epsilon_0 = 80.0$ for pure water at 300 K.

Here, the computed ϵ_0 values for 1-octanol are net lower than the experimentally observed ϵ_0. Considering the ratio of ϵ_0-(computed) to ϵ_0(experimental) (approximately 5/8), one might argue that the model is not doing so well in reproducing this liquid trait. This result may well be attributable to insufficient sampling, or perhaps the limitations of microscopic system size, or possibly to approximations in the octanol model and its parameterization. Also, the effect of neglecting electronic and distortional polarizations may figure significantly in the low dielectric octanol. Recall that only the reorientational contribution to ϵ_0 has been computed. One might make a strictly nonrigorous case for simply adding in the experimentally known contribution of the optical component, an extra $2.15 - 1.0 \approx 1.1$ to each calculated ϵ_0, giving computed values of 6.2 and 5.3 for 40 and 75 °C. While the absolute value of ϵ_0 was not perfectly reproduced, the simulations do faithfully reproduce a qualitatively correct low-dielectric media, yet one which is not totally nonpolar. The correct temperature dependence is also reproduced, a trend toward a lower static dielectric constant as temperature increases.

Frequency-dependent dielectric behavior provides information about the reorientational dynamics of a liquid media. Each of the three characteristic relaxations of long-chain *n*-alkanols is associated with some dynamic motion or rearrangement event in the media. Although experimentalists have reached a general consensus regarding the molecular motions responsible for the faster relaxations τ_2 and τ_3 in *n*-alkanols, the nature of the

(69) Neumann, M. *J. Chem. Phys.* **1986**, *85*, 1567.
(70) Watanabe, K.; Klein, M. L. *Chem. Phys.* **1989**, *131*, 157.
(71) Reddy, M. R.; Berkowitz, M. *Chem. Phys. Lett.* **1989**, *155*, 173.
(72) Alper, H. E.; Levy, R. M. *J. Chem. Phys.* **1989**, *91*, 1242.
(73) Bertolini, D.; Cassettari, M.; Salvetti, G. *J. Chem. Phys.* **1982**, *76*, 3285.

Table 7. Pure Liquid 1-Octanol Static Dielectric and Relaxation Time Analysis[a]

	40 °C				75 °C			
property	expt	%contrb	comput	coeff	expt	%contrb	comput	coeff
τ_1 (1-exp fit)			176.0	(89.)			38.0	(87.)
τ_1 (3-exp fit)	664.0	(85.3)	207.0	(83.)	162.0	(75.)	55.0	(70.)
τ_2 (3-exp fit)	29.5	(8.8)	6.6	(11.)	15.8	(15.)	9.6	(19.)
τ_3 (3-exp fit)	2.7	(5.9)	0.4	(5.)	1.9	(10.)	0.7	(9.)
ϵ_0	8.7		5.1		6.1		4.2	

[a] Experimental (expt) and computed (comput) relaxation times τ_r (in picoseconds) and static dielectric constants ϵ_0 are reported at two temperatures. The percent contributions that each τ_r makes to the overall dielectric relaxation are given in parentheses (%contrb and coeff). Decay curves were computed over 2.0 ns (40 °C) or 3.3 ns (75 °C) trajectories. The single-exponential function was fit to 400 ps segments of $C(\mathbf{M}^2(t))$ decay curve. The triple-exponential fit was to 30.0 ps segments of the decay curve. ϵ_0 was computed over 2.0 ns (40 °C) or 3.3 ns (75 °C). Experimental ϵ_0 and τ values were taken as the average of those from refs 46 and 77. The 75 °C "experimental" ϵ_0 values were linearly extrapolated from actual experimental data at 20, 40, and 60 °C (correlation coefficient $r = 0.999$). Experimental %contrb values are computed using experimental values for ϵ_{01}, $\epsilon_{\infty 1}$, and $\epsilon_{\infty 2}$, from ref 77 and use of $\epsilon_{\infty 3} \approx 2.1$ from ref 46. The values of τ at 75 °C were computed by first converting τ at 20, 40, and 60 °C into activation free energies $\Delta F^{\ddagger}$ through Eyring's linearizing formula $\tau = h/(k_B T) \exp[-\Delta F^{\ddagger}/RT]$, extrapolating $\Delta F^{\ddagger}$ to 75 °C ($r = 0.998$), then computing back through the formula to get τ(75 °C).

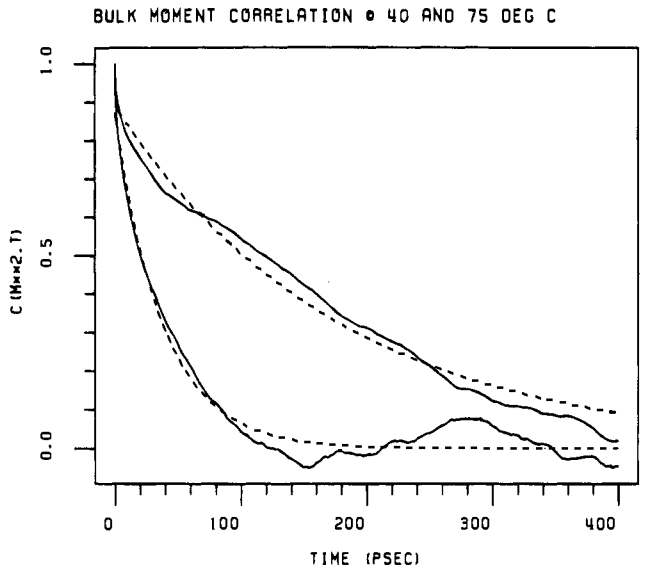

Figure 19. Plots of the autocorrelation of the bulk polarization moment fluctuations, $C(\delta\mathbf{M}(t))$, as in eq 6, for pure 1-octanol at 40 °C (upper solid line) and 75 °C (lower solid), over lag times up to 400 ps. The broken lines show the single-exponential fits to the raw data.

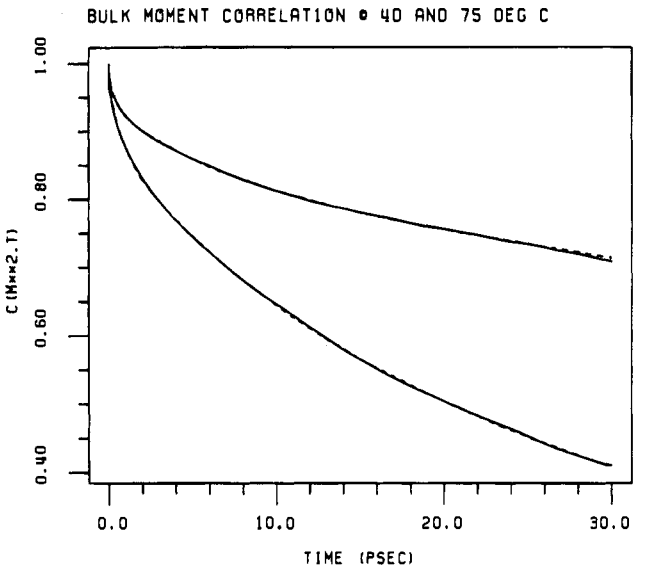

Figure 20. Plots of the autocorrelation of the bulk polarization moment fluctuations, $C(\delta\mathbf{M}(t))$, as in eq 6, for pure 1-octanol at 40 °C (upper solid line) and 75 °C (lower solid), over lag times up to 30 ps. The superimposed broken lines show the triple-exponential fits to the raw data.

molecular level event responsible for the slowest relaxation time τ_1 has long stood in question. Can our new found knowledge of octanol's internal structural details help to suggest a plausible mechanism for this slow relaxation?

The dielectric relaxation behavior exhibited by the modeled octanol was characterized by computing the time autocorrelations of the bulk dipole moment fluctuations $C(\delta\mathbf{M}(t))$ using the algorithm described by Allen and Tildesley.[74] Correlation lags (time multiples of 0.04 ps) of lengths up to 400 ps were taken along the 2.0 ps (40 °C) or 3.3 ps (75 °C) trajectories. Lags points were initiated and followed from each saved coordinate set. All values for lags of the same length were then averaged for each temperature. Also, for short-time response, lags (time multiples of 0.006 ps), of lengths up to 50.0 ps were computed. Figure 19 displays plots of $C(\delta\mathbf{M}(t))$ at 40 °C (upper solid line) and 75 °C (lower solid line), shown fitted with single exponentials (broken lines) over 400 ps blocks by using the Levenberg–Marquardt nonlinear least-squares-fitting method.[75] Correlations decay within 100–200 ps for the 75° trajectory (lower curve), beyond which the curve oscillates about the zero line.

Values for τ_1 and the pre-exponential coefficient A_1 (see eq 6 above) are reported in Table 7. The error in $C(\delta\mathbf{M}(t))$ progressively increases in the direction of increasing time as data become more sparse. The statistical accuracy over short times is much greater. The shorter time τ_2 and τ_3 relaxations (and an alternative value for τ_1) were obtained from triple-exponential fits to 30 ps blocks within the 50 ps maximum lag period analyses. The short-time decays (solid lines) and their fits (broken lines) are plotted in Figure 20. Table 7 lists the τ_r and A_r values obtained.

The value of τ_1 obtained from this fitting to a single exponential (176 ps at 40 °C and 38 ps at 75 °C) can be regarded as qualitatively representing the decay of long-term fluctuations in $\mathbf{M}$ and thus the long-term reorientation dynamics of the media. The single-exponential fit is influenced most heavily by the slowest relaxation mechanism. The root mean squares of deviation (RMSDs) between the 400 ps decay plots and their fitted exponential curves (in Figure 19) are 12.8 (40 °C) and 13.3 (75 °C). The faster relaxations are masked due to statistical uncertainty. The degree of error in the autocorrelations can be estimated by a visual appraisal of the waviness seen in the 400 ps curves and the magnitude of the oscillations about the zero line in Figure 19.

Triple-exponential fitting of the decays leads to results that are encouraging in that the relative relationships between τ_1,

(74) Allen, M. P.; Tildesley, D. J. *Computer Simulation of Liquids*; Clarenden Press: Oxford, U.K., 1987; p 186.

(75) Press, W. H.; Flannery, B. P.; Teukolsky, S. A.; Vetterling, W. T. *Numerical Recipes, The Art of Scientific Computing*; Cambridge University Press: Cambridge, 1989; Chapter 14.

τ_2, and τ_3 are reproduced by the simulation. The three relaxation times each have about 1 order of magnitude between them as computed or measured experimentally (refer to Table 7, e.g. at 75 °C the three reorientational decay times are computed to be 55.0, 9.6, and 0.7 ps and measured as 162.0, 15.8, and 1.9 ps). In Figure 20, the fit curves (broken lines) essentially superimpose onto the decay plots (solid lines); the RMSDs between the decay plots and fitted curves are 0.002 (40 °C) and 0.012 (75 °C). In the absolute sense, the simulation dynamics affecting dielectric relaxation are 3−6 times more rapid (40 °C), or 2−3 times more rapid (75 °C, better converged), than that measured by experiment. Because no explicit hydrogens are attached to the carbons, intermolecular friction/entanglement is expected to be significantly reduced. This is the most likely cause of the discrepancy between the MD simulation and experimental results.[76]

The relative contributions of each molecular relaxation to the overall dielectric response are available from experimental data;[46,77] they are presented in Table 7 as %contrb. These values should be compared with the values of the coefficients A_r computed from eq 6 above, reported under coeff in Table 7. The percent contributions of each relaxation mechanism are extremely well reproduced in the pre-exponential coefficients A_r, (e.g., at 75 °C compare the percent contribution that each reorientation makes as experiment/computed: 75/70, 15/19, 10/9). The model media also produces the correct trend with respect to temperature; the faster relaxation mechanisms make a greater relative contribution to the decay as the barrier to τ_1 is overcome at increased temperatures.

A. τ_3 Relaxation Mechanism. Investigators agree that the picosecond time scale relaxation τ_3 is due to the rotational motion of free hydroxyl groups. The low $\Delta H^{\ddagger}$ transition barrier height associated with the process, about 1.0 kcal/mol, is identical with the barrier height hindering hydroxyl rotation (from microwave spectroscopy).[78] The dipolar H−O−C−C group's rotation about the O−C bond at the rate of about 10^{12} s^{-1} is about 1 order of magnitude slower than a slow molecular vibration. This is apparently the only molecular motion in the system which could account for the τ_3 dielectric relaxation. Because only 5−6% (on average) of the hydroxyls are *free*, the overall contribution should be small. Notice the agreement between experiment and simulation in Table 7 regarding the percentage contribution made by τ_3 to the overall dielectric relaxation; headings %contrb and coeff are near 5−10%. The computed τ_3 (0.4 ps at 40 °C, 0.7 ps at 75 °C) decays more rapidly than experimental observations (2.7 ps at 40 °C, 1.9 ps at 75 °C). Yet, at about 1 ps the computed τ_3 is of the correct order of magnitude.

B. τ_2 Relaxation Mechanism. The second most rapid dielectric relaxation mechanism, τ_2, spans 10 to several tens of picoseconds, on a time scale corresponding to the rotation of an entire molecule or perhaps the rotation of a small complex of two or three molecules.[46,77,79−81] Consistent with this explanation, single molecules (or small complexes) rotate, change their conformational shape, and generally contort themselves to obtain new orientations within their temporary surrounding media cages in the slowly deforming viscous media. Experimentalists believe the molecular event responsible for this relaxation does not require the breakage of hydrogen bonds, since it occurs on a more rapid time scale than that required on average for hydrogen-bond turnover (which will be discussed in detail later). Considering the hydrogen-bonded polymeric chains in 1-octanol, it is possible that τ_2 could also involve twisting and rotating of the end-of-chain species. For this group of molecules bound by only a single hydrogen bond, dipoles could change direction and magnitude without hydrogen-bond breakage, thus making a low-percentage contribution to $\delta\mathbf{M}$.

Consider, however, that if the τ_2 relaxation occurs over a time scale that is longer than that required for the turnover of unpaired monomers, then it would not be completely accounted for simply on the basis of monomer rotations. Monomers would not be enduring long enough for "rate-limiting" rotations to take place. In that case, τ_2 could be due to the reorientation of rapidly reorienting small complexes such as dimers or trimers or to the reorientation (without breakage) of singly-hydrogen-bonded end-group species. This is essentially the consensus rationale presented in the literature up to this point in time.

The decay time for the survival of completely unpaired species, monomers, was computed from MD trajectory data. At some initial time t_0 there is a set of free monomers $\mathbf{F}_i$ which can be identified. As time progresses, each member of this set of monomers will gradually become hydrogen bonded, forming some complexed species. In one relaxation time for monomer decay, about one-half the monomers do not survive; they become bound. Assuming exponential decay, the time autocorrelation of unpaired monomers can be represented by the formula

$$C(\mathbf{F}_i(t)) = \frac{\sum_i F_i(t_0)\, F_i(t_0 + t)}{\sum_i F_i(t_0)} = A e^{-(t/\tau_F)} \qquad (10)$$

where τ_F is the free monomer "annihilation".

The decay curves (not shown) for pure 1-octanol monomer annihilation were fitted to single exponentials giving τ_F(40 °C) = 4.1 ps and τ_F(75 °C) = 4.7 ps with RMSDs of 0.20 and 0.31, respectively. But the dielectric relaxation times from the MD are τ_2(40 °C) = 6.6 ps and τ_2(75 °C) = 9.6 ps (as reported in Table 7). Monomers are annihilated extremely rapidly and within about the same time as the τ_2 relaxation mechanism occurs. Of course, new (reorientable) monomers are being created at exactly the same rate. But, we shall see in the next section that on average hydrogen-bond turnover takes 1 order of magnitude longer than this. Apparently there is a small population of weakly bound itinerant (monomeric or soon to become monomeric) molecules (5−10%) which exchange hydrogen bonds at a much more rapid rate than the average. These would be the peripheral molecules, those that are breaking away from or binding onto the ends of chains, or those that wander at the outskirts of an otherwise stable structure such as a micellar aggregate. Prior to these MD simulations, this phenomena has not been described in octanol. This finding suggests that some mechanism other than simple monomer or small species rotation could be responsible for the τ_2 relaxation. It may be that the rapid exchange and concomitant reorientation of itinerant monomer molecules directly contributes to the τ_2 relaxation.

C. τ_1 Relaxation Mechanism. Experimentalists have proposed various hypotheses to explain the τ_1 relaxation of several hundreds of picoseconds. So far, τ_1 has eluded description at the molecular level. Experimentalists generally offer a mechanism involving intermolecular cooperativity, some relatively obscure collective motion. Investigators disagree as to whether τ_1 is governed by hydrogen-bond breakage, although

(76) Bareman, J. P.; Klein, M. L. *J. Phys. Chem.* **1990**, *94*, 5202. Muller-Plathe, F. *J. Chem. Phys.* **1992**, *96*, 3200.
(77) Gestblom, B.; Sjöblom, J. *Acta Chem. Scand., Ser. A* **1984**, *38*, 47.
(78) Mizushima, S. *Structure of Molecules and Internal Rotation*; Academic Press Inc.: New York, 1954.
(79) Semulon, H. A. *Proc. IRE* **1951**, *39*, 175.
(80) Dannhauser, W.; Flueckinger, A. F. *Phys. Chem. Liq.* **1970**, *2*, 37.
(81) Glasser, L.; Crossley, J.; Smyth, C. P. *J. Chem. Phys.* **1972**, *57*, 3977.

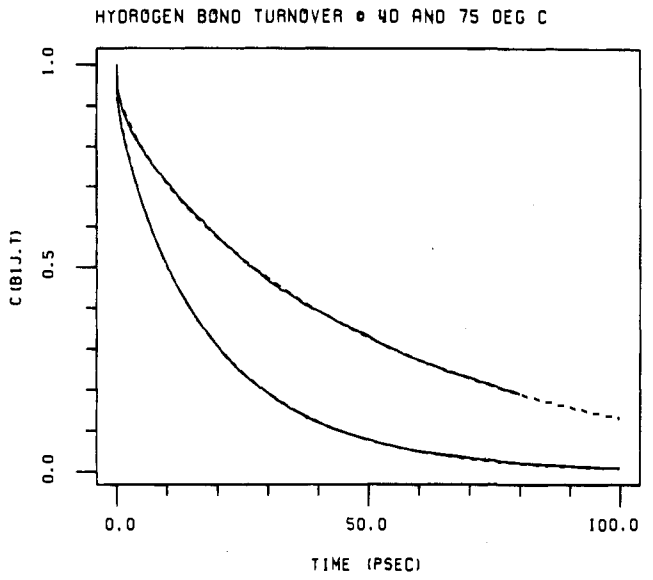

Figure 21. Plots of hydrogen-bond decay or "annihilation" in pure 1-octanol at 40 °C (upper lines) and 75 °C (lower lines). Double-exponential fits (broken lines) are superimposable over the raw data (solid lines).

most believe this cannot be the rate-limiting step;[77] the free-energy barrier for the τ_1 mechanism is a bit higher than that for hydrogen-bond breakage. However, examination of a set of octanol isomers with the hydroxyl placed at various locations along the alkane chain clearly shows that τ_1 is dependent on the placement of the hydrogen-bonding group.[82,83] In octanol isomers where the hydroxyl group is sterically hindered by neighboring hydrocarbon groups, no τ_1 relaxation was observed. Further, a study of a series of *n*-alkanols of increasingly longer alkyl chains shows that τ_1 is also at least partially a function of chain length; τ_1 increases with chain size.[83] τ_1 must be due to a complex orientational rearrangement of dipolar groups which depends on the entire molecule, both the hydroxyl and the chain, and also likely involves interactions between multiple molecules. Knowledge of 1-octanol's several tiers of internal structure suggests that to understand this aspect of the media's internal dynamics one might look to the next highest category of structural complexity beyond individual molecules and their nearest adjacent hydrogen-bonding neighbors. One might consider the reorientational dynamics at the level of molecular aggregates.

Let us propose that τ_1 is the result of the overall restructuring of the media through the simultaneous breakdown and reformation of the various aggregate species. In a static electrical field, the final structure would be driven to optimize the alignment of the individual polarizable elements in the field, at once increasing the bulk dipole moment and the free energy of the media. When the field is then removed, thermally driven motion causes a complex reorientational event; hydrogen-bonded chains and ring clusters forming the aligned aggregates "turnover". The turnover rate for aggregates is governed by their ability to break and exchange hydrogen bonds, untangle their chains, reconform, shift position, rotate, undergo diffusion, and reform micelles, until the media is overall structurally reconfigured to give a net time-averaged moment $\langle \mathbf{M} \rangle_{\text{time}} = 0$. Is the rate of *aggregate turnover* consistent with the slow relaxation time τ_1?

D. Hydrogen-Bond Lifetimes. A treatment of that question must first rule out simple hydrogen-bond turnover as the mechanism responsible for τ_1. Over time, an initial set of hydrogen bonds formed at $t(0)$ will break due to collisions and exchanges. Simultaneous with the destruction of the $t(0)$ hydrogen-bond set, a new set is forming. At some time t in the future, none of the original hydrogen bonds will have survived; the new set will be totally uncorrelated with that at $t(0)$. Progressive changes in the hydrogen-bonding configuration will be reflected in the fluctuations of the bulk dipole moment **M**. Time-autocorrelation decay curves for hydrogen-bond endurance can be generated via the method described by Rapaport.[84]

A quantity $B_{ij}(t)$ is defined to have a value of unity if molecules i and j are hydrogen bonded at time t and a value of zero if no bond is present. The set of values $\mathbf{B}_{ij}(t)$ for all hydrogen-bonded pairs describes the hydrogen-bonding configuration at a given instant t. Each initial pair $B_{ij}(t=0)$ is monitored through the time course of the MD trajectory until it breaks at time t; at this point $B_{ij}(t)$ makes the transition from unity to zero. The time-autocorrelation function takes the form

$$C(\mathbf{B}_{ij}(t)) = \frac{\sum_{ij} B_{ij}(t_0)\, B_{ij}(t_0 + t)}{\sum_{ij} B_{ij}(t_0)} = A e^{-(t/\tau_B)} \qquad (11)$$

where the decay time constant τ_B, an indicator of continuous hydrogen-bond lifetime, is defined assuming the decay of $C(\mathbf{B}_{ij}(t))$ is exponential.

The set $\mathbf{B}_{ij}(t)$ at the beginning of each of twenty-five (non-overlapping) 80 ps trajectories (40 °C), or thirty-nine 100 ps trajectories (75 °C), were taken as $t(0)$. The multiple decay samples, each containing 250 molecules, were then averaged to give $C(\mathbf{B}_{ij}(t))$ at each temperature. A geometric definition of the hydrogen bond was used here; when the heavy atom O−O distance exceeds 3.7 Å, the hydrogen bond is broken. Further, a bond may become severed yet not considered permanently broken unless it *remains* severed for a specific period; bonds reformed within 0.5 ps are considered as unbroken.

Figure 21 shows time-autocorrelation decays for hydrogen-bond lifetimes or "endurance" times (solid lines) along with their double-exponential fit functions (broken lines). Two contributions, τ_a and τ_b, to the decay of hydrogen bonds were extracted. The pre-exponential coefficients are taken as percentage contributions. At 40 °C, 82% of the decay is due to $\tau_a = 54.5$ ps; another 11% is due to a minor contributor $\tau_b = 6.6$ ps. At 75 °C, 76% of the decay is due to $\tau_a = 21.8$ ps; another 16% is due to the minor contributor $\tau_b = 4.9$ ps. The fit is excellent with RMSDs of 0.015 (40 °C, upper lines) and 0.013 (75 °C, lower lines), respectively. The computed τ_a turnover rate for hydrogen bonds is thus significantly faster than the slowest dielectric relaxation time computed from the model ($\tau_1 \approx 176-207$ ps at 40 °C, and $\tau_1 \approx 40-55$ ps at 75 °C) as reported in Table 7. In view of this, it would appear to be unlikely that simple hydrogen-bond turnover could be the rate-limiting event ultimately responsible for the slow τ_1 dielectric response.

Note also the magnitude of the secondary mechanism contributing to hydrogen-bond decay. Hydrogen bonds break via the τ_b mechanism at about the same rate as was computed earlier for the annihilation of free monomers. τ_b must reflect monomer "creation". It is reassuring that a process making a minor contribution to the calculated hydrogen-bond breakage time is consistent with the hydrogen-bond formation time computed by directly observing monomer annihilation (recall τ_F was 4.1 and 4.7 ps at 40 and 75 °C, respectively). This lends further credence to our earlier proposal of a small set of itinerant

(82) Crossley, J.; Glasser, L.; Smyth, C. P. *J. Chem. Phys.* **1971**, *55*, 2197.
(83) Shinomiya, T. *Bull. Chem. Soc. Jpn.* **1989**, *62*, 908; 3636.
(84) Rapaport, D. C. *Mol. Phys.* **1983**, 1151−62.

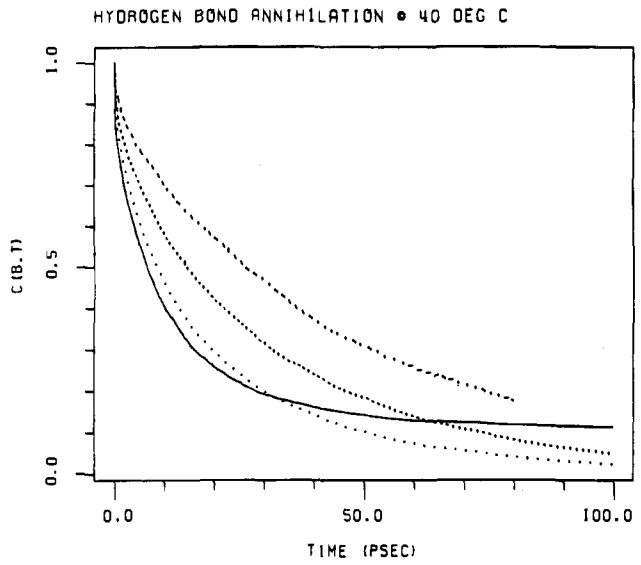

Figure 22. Plots of hydrogen-bond decay or "annihilation" in water-saturated 1-octanol at 40 °C. The uppermost line (long dashes) for pure 1-octanol is shown for comparison. The second highest line (short dashes) is for octanol−octanol hydrogen bonds; the third highest line (dotted) is for octanol−water bonds; the solid line is for water−water hydrogen bonds.

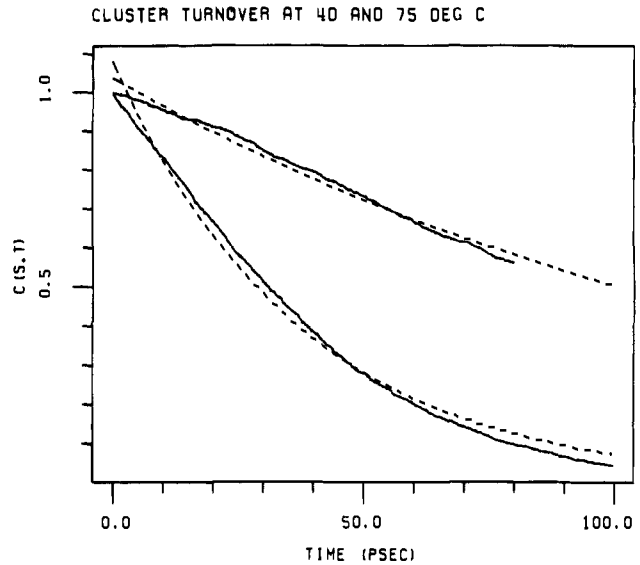

Figure 23. Plots of aggregate-cluster decay or "annihilation" in pure 1-octanol at 40 °C (upper lines) and 75 °C (lower lines): single-exponential fits (broken lines) to the raw data (solid lines).

molecules which rapidly exchange hydrogen bonds, reorienting in the process, influencing the bulk moment fluctuations.

Figure 22 reports hydrogen-bond decays in water-saturated 1-octanol at 40 °C. The uppermost line (long dashes) describes hydrogen-bond decay in (pure liquid) 1-octanol at 40 °C, shown for comparison. The second-highest curve (short dashes) is for octanol-to-octanol hydrogen-bond breakages (in hydrated octanol media). The turnover is more rapid in the presence of saturating waters. The third highest curve (dotted) is for octanol-to-water bond breakage, and the solid curve is for water-to-water hydrogen-bond breakage. Hydrogen bonds involving waters are exchanged most rapidly. However, notice the long-term behavior of some water-to-water hydrogen bonds. While some water−water bonds are the most rapidly exchanging of all, another set of water−water bonds are the most stable of all in the system (evidenced by the long tail of the solid curve). One might speculate that these enduring water−water hydrogen bonds could involve the relatively few molecules lodged tightly within the core of inverted micellar aggregates.

E. Microstructure Turnover. Are the long-term fluctuations of the bulk dipole moment directly correlated to the evolution of the microstructure configuration? If the turnover rate for microstructural configurations is equivalent to the rate of decay of long-term fluctuations in **M**, then we might associate this molecular-level process with the macro-level τ_1 dynamic relaxation. Let us determine whether the two processes share the same long-term rate of decay. Just as the internal structure can be characterized on one level by identifying distinct microstructures (hydrogen-bonded polymeric chains, clusters, and micellar aggregates) as described here earlier, the turnover rate of these structures can be determined by computing the time correlation of their annihilation, as was done for hydrogen bonds. At any time t, say $t = 0$, there exists a uniquely configured set of identifiable microstructures $\mathbf{S}_m(0)$. At some future time, the ensemble of microstructures composing $\mathbf{S}_m(t)$ will be entirely uncorrelated with those at $\mathbf{S}_m(0)$. Although individual molecular positions may have changed only nominally, the formation of a renewed network of microstructures may grossly alter the overall hydrogen-bonding configuration, giving rise to a new instantaneous direction and magnitude for **M**. While correlation does not prove cause and effect, the explanation could be consistent and physically reasonable in the light of our newly enhanced understanding of octanol's internal structure.

The calculation was carried out exactly as described above for hydrogen-bond lifetimes, except that clusters rather than bonds are the microstructural entities "turning over". An aggregate cluster of molecules is considered annihilated when the hydrogen bonds originally connecting it together have *all* undergone breakage. The time-autocorrelation function for the decay of aggregates takes a form very similar to hydrogen-bond lifetime decay. Simply substitute $\mathbf{S}_m$ for $\mathbf{B}_{ij}$ and τ_m for τ_B in eq 11, where the decay-time constant τ_m, an indicator of continuous aggregate lifetime, is defined assuming the decay of $C(\mathbf{S}_m(t))$ is exponential.

Figure 23 shows the decay of $C(\mathbf{S}_m(t))$ at 40 °C (upper solid line) and 75 °C (lower solid line) along with single-exponentially-fit functions (broken lines). The computed decay times are τ_m(40 °C) = 138.2 ps and τ_m(75 °C) = 37.3 ps. Although the RMSDs of the fits were 0.20 and 0.71, respectively, it is not unlikely that the value of 138.2 ps in particular would change somewhat if more extended data were available at 40 °C. The pre-exponential coefficients are both 1.0; no improvement in fitting was possible by using multiple exponentials. In the most convergent simulation, the 75 °C study (lower line in Figure 23), the cluster turnover time is almost identical to the computed τ_1 relaxation time (37.3 versus 38.0 ps). In the 40 °C simulation, the cluster turnover time accounts for about 80% (138.2 versus 176.0 ps) of τ_1. As $1/e$ of the clusters have *completely* dissociated within one relaxation time period, i.e 37.3 ps at 75 °C, it is probable that relatively thorough mixing occurs over the 3.2 ns trajectory. It was found (not illustrated here) that wholly new combinations of molecules (clusters) are formed many times over during the MD trajectories.

Figure 24 simultaneously displays four different time-correlation functions, all for pure 1-octanol at 75 °C: $C(\mathbf{M}(t))$, $C(\mathbf{S}_m(t))$, $C(\mathbf{B}_{ij}(t))$, and $C(\mathbf{F}_i(t))$. Between 0.0 and 50 ps, the bulk polarization (solid line) extrapolates between the decay curves for shorter-term processes, namely individual hydrogen-bond breakage (short dashes), and longer-term processes, the turnover of aggregate microstructures (upper long dashes). But notice how the correlation of bulk moment fluctuations overlaps the turnover of aggregate clusters in the long term. These results support our proposal that the τ_1 relaxation time is due to the

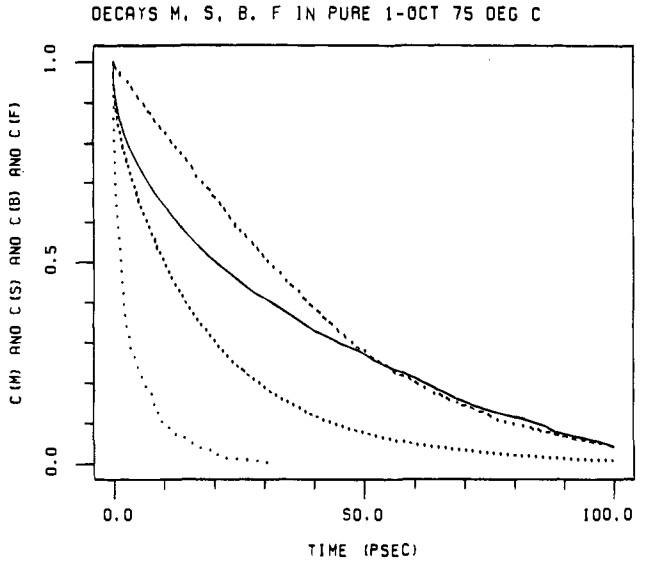

Figure 24. Plots of four different decays in pure 1-octanol at 75 °C, (from raw data): time autocorrelation of bulk moment fluctuations $\delta\mathbf{M}$ (solid line), aggregate-cluster decay $\mathbf{S}_m$ (upper long dashes), hydrogen-bond decay $\mathbf{B}_{ij}$ (short dashes), and free monomer decay $\mathbf{F}_i$ (dotted).

overall restructuring of the media via the simultaneous breakdown and reformation of the various aggregate species.

F. Direct Dependence of $\delta\mathbf{M}(t)$ on Aggregate Turnover. While the data shows correlation of $\delta\mathbf{M}$ with microstructural restructuring events by virtue of their shared time scales, we have not directly demonstrated cause and effect. We have not *proven* that cluster turnover is the mechanism responsible for τ_1. But, the most reasonable alternative mechanism, simple hydrogen-bond turnover; has been ruled out. In order for any process to make a significant contribution to the dielectric relaxation, it must involve a drastic rearrangement of the polarizable moieties, namely the alkoxyl groups. Other possible explanations for the molecular mechanism responsible for the τ_1 relaxation would require arguing for an intra-aggregate or inter-aggregate reorientational mechanism which does *not* involve hydrogen-bond breakage. Because the cluster decay time (which requires the annihilation of all intra-aggregate hydrogen bonds) occurs on approximately the same time scale as the τ_1 relaxation, no such argument could be made. The clusters do not survive long enough to accommodate such a process. Therefore, it is likely that the turnover and concomitant reorientation of the molecules constituting the aggregate microstructures in 1-octanol is the very mechanism responsible for the τ_1 relaxation.

VI. Summary and Conclusions

Hydrated 1-octanol has long been the definitive model for the hydrophobic biophase component in partitioning studies involving drugs and molecules of biological interest. Although not a perfect model for micelles or biomembranes, it contains both polar and nonpolar functionalities characteristic of these more complex structures. These molecular dynamics (MD) simulations have provided a detailed and comprehensive molecular-level picture of the internal structure and dynamics of liquid 1-octanol, its water-saturated solution, and the nature of its interactions with simple solutes. We have described the distribution of the various microstructures present in 1-octanol and demonstrated their influence upon the dynamic motions which give rise to the macroscopic dielectric response of the media.

It was found that OPLS united-atom interaction potentials[21] for hydrocarbons and alkanols developed under a Monte Carlo regime adapted very readily to molecular dynamics as carried out with the potential function used here in the program AMBER. The main differences in model representation by AMBER versus the original OPLS are the allowance for flexible (AMBER) versus rigid (OPLS) bond angles and usage of the same nonbonded 6−12 parameters (AMBER) for intra- and intermolecular interactions versus separate sets of nonbonded 6−12 parameters (OPLS) for intra- and intermolecular interactions. Despite these differences, after minor interaction parameter modifications of the OPLS model, experimentally measured thermodynamic and structural data were very well reproduced by MD simulations with AMBER. These included liquid densities and heat of vaporization for hexane, octane, 1-octanol, and water-saturated 1-octanol, the percentages of various conformers in liquid hexane, the percentage of unbound hydroxyl hydrogens in liquid 1-octanol, the local mole fractions expected due to preferential self-solvation in water-saturated 1-octanol, reproduction of the relative partition coefficients of benzene and phenol in water-saturated 1-octanol, and the reproduction of three relaxations each correctly separated by about 1 order of magnitude in 1-octanol. It was found that the presence of saturating waters increased the rate of diffusion of 1-octanol molecules. Beyond confirmation of the molecular models, an indication that systems have reached equilibration is provided when one considers the simultaneous close agreement with experiment for so many properties.

While qualitatively correct relative trends in dynamic properties were reproduced, the computed dynamics are more rapid in their absolute magnitudes than experimental observations, probably due to the absence of explicit hydrogens in the united-atom model. One would expect absolute relaxation times to be more accurately represented with an all-atom model. However, the united-atom model was chosen over an all-atom model specifically because it facilitates more thorough sampling via long-time-spanning (multi-nanoseconds) MD simulations. If an all-atom model had been employed, with 27 rather than 10 atom centers in 1-octanol, the time of the calculations would have been dramatically increased, as the ratio 27/10 to some power between 1 and 2. Using an all-atom model, investigation of dielectric response mechanisms would have been very difficult at this time, even given generous computer resources. We chose the united-atom model as the most efficient model possible, giving an acceptable degree of realism, sufficient to enable us to investigate liquid-phase reorientational phenomena correlated over long times.

From the MD sample of configurations, it was determined that 1-octanol contains a distribution of various sizes of hydrogen-bonded "polymer" species, both chains and closed rings (Figures 3 and 4). At first glance, the radial pair distribution function (e.g., oxygen-to-oxygen in Figure 8) of 1-octanol is perhaps astonishing, but then completely reasonable when one understands how it reflects the media's internal structure. The hydroxyl oxygens "see" a high concentration of other oxygens in the nearest solvation shell within about 5 Å, then a deficit of oxygens in more distant shells between 5 and 15 Å, but then again a higher than average concentration of oxygens in far shells 15−20 Å away. This leads to the picture of preferentially polar or nonpolar regions in the media due to the formation of inverted micellar aggregates of diameter about 18.5−21.5 Å with hydrophilic cores about 7.75−10 Å across, as illustrated in Figures 5, 13, and 14 (where numbers at the ranges' high ends apply to water-saturated 1-octanol).

New insights have been gained into the mechanisms responsible for 1-octanol's three dielectric relaxations. The model incorporated a long-range reaction field to facilitate the calculation of the macroscopic dielectric behavior of the pure condensed phase at 40 and 75 °C. Qualitative agreement with experimental

values is obtained for the static dielectric constant; ϵ_0 is calculated as 5.1 (8.7 experimental) at 40 °C and as 4.2 (6.1 experimental) at 75 °C. An examination of frequency-dependent dielectric response led to the association of dynamic molecular-level events with correlated dielectric relaxation times as computed for the model liquid. Experimental dielectric relaxation measurements have previously been fit to a model involving three decay times, at both 40 and 75 °C. The results of these MD calculations are consistent at both temperatures, agreeing in relative trends and percentage contribution for each mechanism, with approximately a factor of 3 underestimate of the absolute relaxation times.

MD results are consistent with the interpretation of experiment regarding the most rapid relaxation process, τ_3, which is on the order of 1 ps. This relaxation likely corresponds to the torsional rotation of the approximately 5% unbound hydroxyl groups in the liquid. A new interpretation of the second relaxation time, $\tau_2 \approx 10-30$ ps, emerges from this study. The extra-rapid breakage and reformation of hydrogen bonds involving "itinerant" molecules at the periphery of larger more stable aggregates may be a contributing mechanism (as opposed to or along with simple molecular rotation, which was previously thought to be the mechanism). Finally, we provide data supporting our proposed hypothesis that the slowest relaxation time, $\tau_1 \approx 100$ to several hundred picoseconds, corresponds to the turnover (breakdown and reformation) of the aggregate structures themselves.

Free-energy perturbation (FEP) calculations on the relative solubilities of benzene and phenol in water-saturated 1-octanol versus pure water were examined, especially with respect to structural aspects of the interaction. The difference in the octanol/water partition coefficients of phenol and benzene were previously computed via the coarse-grain parallel processing FEP approach developed in this lab.[36] MD trajectories over several nanoseconds gave apparently convergent values for the relative solvation free energies, which were then converted into the relative partition coefficient $\Delta\log(K_{O/W})$. The agreement between calculated and experimentally determined values for the partitioning of an aromatic hydroxyl was excellent (0.76 ± 0.39 calculated versus 0.67 experimental). Using molecular configurations saved from the trajectory generated during the FEP study, the orientation of the solutes with respect to their hydrated-octanol solvation-shell structures were described in detail here. On the basis of the structural analyses, we postulate that water-saturated 1-octanol's capability to serve as a biophase analog is due to the formation of preferentially polar versus nonpolar regions in the media, crudely mimicking the components, and perhaps compartmental boundaries, found in the body.

Acknowledgment. We are grateful to the National Science Foundation (CHE-91-13472) and National Institutes of Health (GM-29072) for research support. We thank the San Diego Supercomputing Center for time allocations on their Cray YMP and nCUBE machines. We also thank the UCSF Computer Graphics Laboratory, R. Langridge, P.I. (RR-1081), and associated personnel for their assistance in creating graphical images.

JA9410606